https://doi.org/10.5194/acp-2020-428
Preprint. Discussion started: 29 May 2020

Atmospheric Chemistry and Physics Discussions

Hygroscopic behavior of aerosols generated from solutions of 3-methyl-1,2,3-butanetricarboxylic acid, its sodium salts, and its mixtures with NaCl

Li Wu[1], Clara Becote[2,3,4], Sophie Sobanska[2], Pierre-Marie Flaud[3,4], Emilie Perraudin[3,4], Eric Villenave[3,4], Young-Chul Song[1], Chul-Un Ro[1*]

[1]Department of Chemistry, Inha University, Incheon, South Korea

[2]Institut des Sciences Moléculaires, UMR CNRS 5255, University of Bordeaux, Talence, France

[3]University of Bordeaux, EPOC, UMR 5805, 33405 Talence cedex, France

[4]CNRS, EPOC, UMR 5805, 33405 Talence cedex, France

Abstract

Secondary organic aerosols (SOAs), which are formed and transformed through complex physicochemical processes in the atmosphere, have attracted considerable attention over the past decades because of their impacts on both climate change and human health. Recently, 3-methyl-1,2,3-butanetricarboxylic acid (MBTCA), a low volatile, highly oxidized, secondary generation product of monoterpenes, is one of the most relevant tracer compounds for biogenic SOAs. Therefore, MBTCA was selected to understand its hygroscopic properties better. In addition, interactions between the organic acid and inorganic components have been reported, which may alter their hygroscopic properties mutually. In this study, laboratory-generated, micrometer-sized, pure MBTCA, mono-/di-/tri-sodium MBTCA salts, and MBTCA-NaCl mixture aerosol particles of four mixing ratios (molar ratios = 1:1, 1:2, 1:3, and 2:1) were examined systematically to observe their hygroscopic behavior by varying the relative humidity (RH) from RH = ~95% to ~1% through a dehydration process, followed by a humidification process from RH = ~1% to ~95%, using in-situ Raman microspectrometry (RMS) assembled with a see-through impactor where the particles were deposited on a Si wafer. The hygroscopic behavior of pure MBTCA and MBTCA-NaCl mixture aerosol particles of three mixing ratios (molar ratios = 1:1, 1:2, and 1:3) were also examined using a levitation system mounted on in-situ RMS through a humidification process from

*Corresponding author. Tel.: +82 32 860 7676; Fax: +82 32 867 5604; E-mail: curo@inha.ac.kr

https://doi.org/10.5194/acp-2020-428
Preprint. Discussion started: 29 May 2020


Atmospheric Chemistry and Physics Discussions

RH = ~10% to ~80% after a quenching process from droplets, followed by dehydration from RH = ~80% to ~10%. The pure MBTCA droplets effloresced at RH = ~30-57.8% and did not dissolve until RH > 95%. The mono- and di-sodium MBTCA salt aerosols did not show clear efflorescence RH (ERH) and deliquescence RH (DRH). In contrast, the tri-sodium MBTCA salt exhibited ERH = ~44.4-46.8% and DRH = ~53.1%, during the hygroscopic experiment cycle. The mixture aerosols generated from solutions of MBTCA:NaCl = 1:1 and 2:1 showed no visible ERH and DRH in the see-through impactor because of the partial and total consumption of NaCl, respectively, through chemical reactions during the dehydration process. The mixture particles with a 1:1 molar ratio in the levitation system exhibited a clear DRH at ~71% and ERH at ~50%. This suggests less reaction between the mixtures and a larger portion of NaCl remaining in the levitation system. The other mixtures of MBTCA:NaCl = 1:2 and 1:3 displayed single-stage efflorescence and deliquescence at ERH = ~45-50% and DRH = ~74%, respectively, because of the considerable amount of NaCl present in the mixture aerosols in both systems. Observations and Raman analyses indicated that only monosodium MBTCA salt aerosols could be formed through a reaction between MBTCA and NaCl. The reaction occurred more rapidly with a more elevated concentration of either MBTCA or NaCl, and the controlling factor for the reactivity of the mixtures depended mostly on the availability of H^+ dissociated from the MBTCA tricarboxylic acid. The lower degree of reaction of the mixture particles in the levitation system might be caused by the relatively airtight circumstance inside, i.e., the less release of HCl. In addition, the quenching process, i.e., the starting point of the hygroscopicity experiments, induced the solidification of MBTCA, and further, a slow reaction between MBTCA and NaCl. The study revealed that the interactions between the MBTCA and NaCl could modify the properties of the organic acid in the atmosphere, leading to enhanced capability of the probable heterogeneous chemistry in the aqueous aerosols.

1. Introduction

Chemical processes, such as gas-phase oxidations of airborne biogenic and anthropogenic volatile organic compounds (VOCs) by ozone (O_3), hydroxyl radical (OH), and nitrate radical (NO_3), and their condensed-phase reactions with preexisting aerosols, can promote the formation of increasingly oxidized and less volatile secondary organic aerosols (SOAs). SOAs are a ubiquitous and dominant fraction of the

https://doi.org/10.5194/acp-2020-428
Preprint. Discussion started: 29 May 2020


Atmospheric Chemistry and Physics Discussions

fine aerosol mass that exists as liquid, amorphous solid, semi-solid, and phase-separated aerosol particles (Jang et al., 2002; Hallquist et al., 2009; Jimenez et al., 2009; Virtanen et al., 2010; Koop et al., 2011; Bateman et al., 2015b; Shrivastava et al., 2015; Bernard et al., 2016; Pajunoja et al., 2016; Freedman, 2017; Shrivastava et al., 2017; Kim et al., 2018; Srivastava et al., 2018; Liu et al., 2019; Slade et al., 2019; Song et al., 2019; Wu et al., 2019a). These aerosols are of critical importance because of their ability to scatter and absorb solar radiation directly, to affect the number of CCN (cloud condensation nuclei) through the formation of new particles and the growth of preexisting particles, and further impact the climate and human health (Haywood and Boucher, 2000; Topping et al., 2013; Poschl and Shiraiwa, 2015; Reid et al., 2018; Marsh et al., 2019). SOAs are highly dynamic, multiphase chemical systems with a range of volatility and solubility and model simulations have claimed that the phase state of SOAs differs according to the global locations and altitudes with an evolving relative humidity (RH), temperature, and particle composition (Kroll and Seinfeld, 2008; Shiraiwa et al., 2017).

Oxidative products of biogenic VOCs, such as monoterpenes (e.g., α- and β-pinene), act as a dominant source of SOAs as they have high emission rates on a global scale and give considerable SOA yields, and they play a central role in new particle formation (Guenther et al., 1995; Lignell et al., 2013; Mutzel et al., 2016; Holopainen et al., 2017). Carboxylic acid-containing organic compounds comprise a large fraction of SOAs in the Northern Hemisphere (Yatavelli et al., 2015). An extremely low-volatile tricarboxylic acid, 3-methyl-1,2,3-butanetricarboxylic acid (MBTCA, $C_8H_{12}O_6$), has become one of the most relevant tracer compound for terpene SOAs (Jaoui et al., 2005; Szmigielski et al., 2007; Zhang et al., 2010; Donahue et al., 2012; Müller et al., 2012; Lai et al., 2015; Sato et al., 2016). In addition, it is also a few well-known compounds with a high O:C ratio that is formed in the oxidation of VOCs (Dunne et al., 2016). MBTCA is a second or later generation reaction product from monoterpenes by the OH-initiated oxidation of pinonic acid (PA) in the gaseous and aqueous phases and even at the air-water interface (Müller et al., 2012; Praplan et al., 2012; Aljawhary et al., 2016; Enami and Sakamoto, 2016). The MBTCA concentrations were found to be positively correlated with temperature because of the enhanced photochemical production of PA by OH radicals with increasing temperature (Hu et al., 2008; Zhang et al., 2010; Gómez-González et al., 2012; Miyazaki et al., 2012). A further reaction between MBTCA and OH radicals can result in CO_2 loss (Kostenidou et al., 2018). MBTCA can also accelerate

https://doi.org/10.5194/acp-2020-428
Preprint. Discussion started: 29 May 2020


Atmospheric Chemistry and Physics Discussions

the new particle formation by effectively stabilizing initial molecular clusters with or without sulfuric acid (Donahue et al., 2013; Elm, 2019). MBTCA was first observed at the Amazon basin and in summer aerosols from Ghent, Belgium (Kubátová et al., 2000; Kubátová et al., 2002). The compound was later found in the USA (Jaoui et al., 2005), Europe (Fu et al., 2009; Kourtchev et al., 2009; Zhang et al., 2010; Yasmeen et al., 2011; Gómez-González et al., 2012; Vogel et al., 2013; Kammer et al., 2018; Vlachou et al., 2019), Japan (Miyazaki et al., 2012), the polar regions (Hu et al., 2013), China (Hu et al., 2008; Ding et al., 2012; Li et al., 2013; Fu et al., 2014; Kang et al., 2018; Hong et al., 2019), and Australia (Cui et al., 2019). In addition, it has been observed in forest, marine, mountainous, urban, and rural aerosols, with its levels ranging from 0.03 to 100 ng/m^3, and the level was generally higher in the fine particle fraction than in the coarse fraction (Zhang et al., 2010).

The ability of the aerosol particles to uptake water in the air is dependent on one of the most important physicochemical properties, i.e., the hygroscopicity (Jimenez et al., 2009; Chu et al., 2014; Tang et al., 2019). Hygroscopicity can help better understand the (i) aerodynamic properties, (ii) cloud-droplet nucleation efficiency, (iii) optical properties, and (iv) physicochemical changes through complicated heterogeneous chemical reactions of aerosol particles with various atmospheric gas-phase species. MBTCA was predicted to partition significantly into aerosol-liquid-water (ALW) (Aljawhary et al., 2016). Therefore, a study on the hygroscopic behavior of MBTCA is important for understanding its phase states better when it interacts with water vapor at different RHs as well as its impacts on the heterogeneous chemical reactions, atmospheric environment, and human health (Parsons et al., 2004; Mikhailov et al., 2009; Bateman et al., 2015a; Freedman, 2017; Slade et al., 2019). Atmospheric particles typically involve complex internal mixtures of organic and inorganic compounds (Shrivastava et al., 2017; Karadima et al., 2019). The interactions between organic and inorganic compounds may alter the chemical compositions of SOAs, which in turn affect their physicochemical properties, such as hygroscopicity (Rudich et al., 2007; Wu et al., 2011; Wang et al., 2015; Jing et al., 2016; Wang et al., 2018). Dicarboxylic acids (DCAs) can undergo reactions with inorganics, such as NaCl, resulting in Cl depletion and HCl liberation (Ma et al., 2013; Li et al., 2017). On the other hand, the interactions between tricarboxylic acids and inorganics have never been investigated.

https://doi.org/10.5194/acp-2020-428
Preprint. Discussion started: 29 May 2020


Atmospheric Chemistry and Physics Discussions

In this study, in situ Raman microspectrometry (RMS) was used to examine the hygroscopic behavior, evolution of the chemical composition, phase states, and microstructures, and chemical reactivity of laboratory-generated, micrometer-sized aerosols generated from a pure MBTCA solution, mono-/di-/tri-sodium MBTCA salt solutions, and MBTCA-NaCl mixture solutions. RMS was assembled with either a see-through impactor, where the particles were deposited on a Si wafer, or a levitation system. The particles on the Si wafer were exposed to a hygroscopic measurement cycle, where they experienced a dehydration process first (by decreasing RH from ~95 to ~1%), followed by a humidification process (by increasing RH from ~1 to ~95%). The particles in the levitation system experienced a humidification process first (by increasing the RH from ~10 to ~80%) after quenching from droplets, followed by a dehydration process (by decreasing RH from ~80 to ~10%). NaCl, one of the major components of marine aerosols, was selected as the inorganic component as it was previously reported that organic acids contributed significantly to Cl depletion through a reaction with NaCl (Laskin et al., 2012). In situ Raman analysis could clearly identify MBTCA and its sodium salts during the hygroscopicity measurement despite NaCl being Raman inactive. To the best of the authors' knowledge, this is the first study on the hygroscopic behavior and chemical reactivity of MBTCA and its sodium salts thus far. The results are expected to promote more precise thermodynamic models (Clegg et al., 2003). The phase transitions were observed by monitoring the size changes together with the Raman spectra evolutions of the aerosol particles as a function of the RH. RMS can provide the aerosol compositions, water contents, molecular interactions, and particle-phase states sensitively. Such data can help understand the hygroscopic behavior of complex aerosol particles better (Lee et al., 2008; Li et al., 2017; Wang et al., 2017). The molecular characterization of organic aerosols can provide better insights into the potential mechanisms of SOA formation and transformation (or aging) (Hallquist et al., 2009). Scanning electron microscopy (SEM)/energy-dispersive X-ray spectroscopy (EDX) mapping was used to examine the elemental composition distribution in effloresced particles.

2. Experimental Section

2.1 Sample preparation

https://doi.org/10.5194/acp-2020-428
Preprint. Discussion started: 29 May 2020


Atmospheric Chemistry and Physics Discussions

Pure 0.3 M solutions of NaCl (>99.9% purity, Sigma-Aldrich) and MBTCA (98%, Toronto Research Chemicals, TCR) were prepared. The mixture solutions of MBTCA and NaCl were prepared with molar mixing ratios of MBTCA:NaCl = 1:1, 1:2, 1:3, and 2:1. Mono-/di-/tri-sodium MBTCA salt solutions were obtained by mixing MBTCA and NaOH (>99.9% purity, Sigma-Aldrich) with molar ratios of MBTCA:NaOH = 1:1, 1:2, and 1:3, respectively. A mixture solution of MBTCA and monosodium MBTCA salt with a molar mixing ratio of 1:1 was prepared as well. Aerosol particles were generated by nebulizing the solutions using a single jet atomizer (HCT4810) on the Si wafer substrates (MTI Corporation, 99.999% purity). The size of the droplets examined at RH > 90% ranged from 1 to 15 μm.

2.2 In situ Raman microspectrometry (RMS) for particles deposited on a Si wafer

During the hygroscopic measurements, in situ RMS was performed under a controlled RH to observe the hygroscopic behavior, structural changes, and chemical compositional variations of the aerosols generated from the solutions. The apparatus consisted of three parts: (A) see-through impactor, (B) Raman microscope/spectrometer, and (C) humidity-controlling system. The Si wafer substrate was mounted on the impaction plate in the see-through impactor. A more detailed discussion of the impactor and humidity-controlling system can be found elsewhere (Gupta et al., 2015). Briefly, the RH inside the impactor was controlled by mixing dry and wet (saturated with water vapor) N_2 gases. The flow rates of total 4 $L \cdot min^{-1}$ of the dry and wet N_2 gases were controlled by two mass flow controllers to obtain the desired RH in the range of ~1−95%, which was monitored using a digital hygrometer (Testo 645). The digital hygrometer was calibrated using a dew-point hygrometer (M2 Plus-RH, GE) to provide RH readings with ±0.5% reproducibility. The Raman spectra and optical images of the aerosol particles were recorded by Labspec6 using a confocal Raman microspectrometer (XploRA, Horiba Jobin Yvon) equipped with a ×50, 0.5 numerical aperture objective (Olympus). An excitation laser with a wavelength of 532 nm and 6 mW power was used, and the scattered Raman signals were detected at specific RHs during the hygroscopic measurements using an air-cooled multichannel charge-coupled device (CCD) detector. The data acquisition time for each measurement was 120 s. The spectral resolution was 1.8 cm^{-1} using 1800 gr/mm. The optical images were recorded continuously in RH = 1% steps with a size of 904×690 pixels during the first dehydration (by decreasing RH from ~95 to ~1%), followed by the humidification (by increasing

https://doi.org/10.5194/acp-2020-428
Preprint. Discussion started: 29 May 2020


Atmospheric Chemistry and Physics Discussions

RH from ~1 to ~95%) experiments using a top video camera assembled in the Raman instrument and processed using an image analysis software (Matrox, Inspector v9.0). The changes in particle size with the RH were monitored by measuring the particle 2-D area in the optical images to generate hygroscopic curves. These curves are represented by the area ratio (A/A_0) as a function of RH, where the 2-D projected aerosol area at a given RH (A) is divided by that at the end of the dehydration process (A_0) (Ahn et al., 2010). All hygroscopic experiments were conducted at room temperature (T = 22±1℃). Aerosol particles generated from a pure NaCl aqueous solution to check the accuracy of the system showed typical hysteresis curves with deliquescence RH (DRH) = 75.5(±0.5)% and efflorescence RH (ERH) = 46.3–47.6%, which are consistent with the theoretical and reported values.

2.3 SEM/EDX X-ray mapping of effloresced particles deposited on Si wafer

SEM/EDX X-ray mapping was performed for effloresced particles to determine the morphology and spatial distribution of the chemical elements after the hygroscopicity measurements of individual particles (Ahn et al., 2010; Gupta et al., 2015). The measurements were carried out using a Jeol JSM-6390 SEM equipped with an Oxford Link SATW ultrathin window EDX detector. The resolution of the detector was 133 eV for Mn Kα X-rays. The X-ray spectra and elemental X-ray maps were recorded under the control of Oxford INCA Energy software. A 10 kV accelerating voltage and 0.7 nA beam current were used, and the typical measuring time for the elemental mapping was five minutes. An elemental quantification procedure, which is well described elsewhere (Wu et al., 2019a), was used for obtaining the elemental concentration.

2.4 In situ RMS assembled with levitation system

The levitation experimental set up consisted of coupling an acoustic (ultrasonic) levitator equipped with an environmental cell to an RMS, as shown in Fig. S1. The theory of acoustic levitation is described in detail elsewhere (Seaver et al., 1989). An ultrasonic levitator was modified (APOS BA 10, Tec5, Germany) to be installed within an environmental levitation cell consisting of two quartz windows, allowing the particle analysis (Seng et al., 2018). Two inlet/outlet valves were used for gas supplies to modify the relative humidity (RH) inside the cell. A sensor (SHT75 Sensirion) was placed into the cell to

https://doi.org/10.5194/acp-2020-428
Preprint. Discussion started: 29 May 2020


Atmospheric Chemistry and Physics Discussions

control the RH and temperature. The RH inside the chamber was controlled by mixing dry and wet Ar gases with a flow rate of 200 mL·min^{-1} in the range of 10-80% (±1%) RH, and the temperature was T = 25±3°C, making the experiments close to static flow conditions. The control of humidity and temperature allows limited droplet evaporation and long-term monitoring of the particles. The RMS measurements were performed with a LabRAM HR evolution confocal spectrometer (Horiba Scientific, S.A) at certain RHs first during humidification and then during dehydration. The instrument was equipped with an ×50, 0.45 numerical aperture Olympus objective (WD = 13.8 mm) and a He-Ne laser (λ = 632.8 nm – 6 mW) with a theoretical lateral resolution of ~2 µm, and a depth of the laser focus corresponding to 16 µm with a Δz limit ≥ ±3 µm. The cell was mounted on an XYZ stage under the objective, allowing an adjustment of the droplet in the optimal position for the measurements. The mean size of the initial droplet injected in the levitator was 80 µm. The Raman spectra and optical images recorded at specific RHs were analyzed similarly to those obtained on the Si wafer.

2.5 Measurement of acid dissociation constants of MBTCA

MBTCA is a tri-carboxylic acid with three acid dissociation constants. To determine the three constants, a 0.02 M, 5 ml MBTCA solution was titrated with a 0.1 M NaOH solution, where the constants were determined based on the Henderson-Hasselbalch equations (Harris, 2012):

$$H_3M + OH^- \rightarrow H_2M^- + H_2O \quad pH = pKa_1 + \log([H_2M^-]/[H_3M])$$

$$H_2M^- + OH^- \rightarrow HM^{2-} + H_2O \quad pH = pKa_2 + \log([HM^{2-}]/[H_2M^-])$$

$$HM^{2-} + OH^- \rightarrow M^{3-} + H_2O \quad pH = pKa_3 + \log([M^{3-}]/[HM^{2-}])$$

where H_3M, H_2M^-, HM^{2-}, and M^{3-} represent aqueous MBTCA, mono-, di-, and tri-sodium MBTCA anions, respectively. The pKa_1, pKa_2, and pKa_3 are the pHs when $[H_3M]$, $[H_2M^-]$, and $[HM^{2-}]$ equal $[H_2M^-]$, $[HM^{2-}]$, and $[M^{3-}]$, respectively, during the acid-base titration. Specifically, when NaOH was added at 0.5, 1.5, and 2.5 ml, the corresponding pHs of the solution are the three constants, which were 3.59, 4.85, and 6.79. Fig. 1 shows the calculated titration curve of MBTCA using the three determined Ka values, which is the same as the experimentally obtained titration data, supporting the validity of the Ka values, which were not reported so far.

https://doi.org/10.5194/acp-2020-428
Preprint. Discussion started: 29 May 2020


Atmospheric Chemistry and Physics Discussions

3. Results and Discussion

3.1 Hygroscopic behavior of pure MBTCA particles

Wet-deposited MBTCA aerosols exhibited three types of hygroscopic behavior. As shown in Fig. 2, during the dehydration process, the exemplar droplets of types 1 and 2 shrank continuously with decreasing RH due to water evaporation until RHs = 58.4% and 40%, and then effloresced promptly at RH = 57.8% and gradually at RH = 39 - 35%, respectively. The effloresced particles maintained their size and shape with further decreases in RH. Whereas, the type 3 aerosols decreased continuously in size without a distinct change from RH = 94% to RH = 3% during the dehydration process. During the humidification process, types 1 and 2 particles kept the same size and shape until RH = ~90%, while type 3 particles experienced a phase change at RH = 36.7% and remained the same until RH = ~85%. Fig. 2 also presents the corresponding optical images and in situ Raman spectra to assess the structural evolution of the MBTCA aerosols during the dehydration and humidification processes. Briefly, Raman peaks at ~1411 - 1420 cm^{-1}, ~1460 and ~2950 cm^{-1}, ~1660 - 1730 cm^{-1}, and ~3420 - 3475 cm^{-1} are for vibrations of C=O from COO^-, CH, C=O from COOH, and OH from water, respectively (Edsall, 1937; An et al., 2016). The redshift of the C=O peak (from COOH) from 1715 to 1660 cm^{-1} with decreasing FWHH (full width at half height), which is consistent with the standard MBTCA crystal, and the irregular shape and rough surface of types 1 and 2 aerosols at RH = 57.8% and 35%, respectively, confirmed that the particles effloresced into a solid phase. The optical images in the inset above the hygroscopic curve of the type 2 particles showed gradual efflorescence at RH = 39 – 35%. The water peak at ~3475 cm^{-1} disappeared as well after the efflorescence. In contrast, type 3 aerosols maintained a circular morphology until RH = 3%, as shown in the optical images in Fig. 2, even though an overlapped C=O (from COOH) peak at 1660 - 1680 cm^{-1} appeared during the dehydration process, and the water peak became undetectable, as shown in the Raman spectra at RHs = 45% and 3%, suggesting an amorphous/solid-state and the presence of an activation barrier or diffusional resistance to homogeneous nucleation required for the crystallization of MBTCA droplets as efflorescence is a kinetically controlled process (Martin, 2000; Freedman, 2017). Previous studies reported that α-pinene SOAs were very likely to exist as a highly viscous semisolid or even glassy state at low humidity (Saukko et al., 2012; Renbaum-Wolff et al., 2013; Berkemeier et al., 2014; Dette et al., 2014; Kidd et al., 2014; Song et al., 2016; Lessmeier et al., 2018). In addition, many

https://doi.org/10.5194/acp-2020-428
Preprint. Discussion started: 29 May 2020


Atmospheric Chemistry and Physics Discussions

organic substances, such as carboxylic acids, carbohydrates, and proteins, tend to form amorphous rather than crystalline phases upon the drying of aqueous solution droplets (Mikhailov et al., 2009). The different behavior of the MBTCA particles can be attributed to different nucleation mechanisms, i.e., homogeneous and heterogeneous nucleation, for pure and impure (seed-containing) MBTCA particles, respectively. A similar situation was reported for NH_4NO_3, $NaNO_3$, and NH_4HSO_4 particles (Lightstone et al., 2000; Hoffman et al., 2004; Gibson et al., 2006; Kim et al., 2012; Jing et al., 2018; Sun et al., 2018; Wu et al., 2019b). The Si substrates used in this study could also facilitate efflorescence (Eom et al., 2014; Wang et al., 2017). During the humidification process, the Raman spectra and morphology remained unchanged for types 1 and 2 particles until RH = ~90%, where a slight change in morphology was observed due to structural re-arrangements by the absorption of moisture on the lattice imperfections (Gysel et al., 2002). Type 3 particles during the humidification process became irregular in shape, and the overlapped C=O (from COOH) peak shifted to 1660 cm^{-1} at RH = 36.7%, as shown in the optical image and Raman spectrum, indicating the formation of solids. With the further increase in RH, particles maintained their size and shape until RH = 85%, where they started to decrease in size due to a re-arrangement in structure. The efflorescence of laboratory-generated particles during the humidification process was reported previously in the NaCl-$MgCl_2$ mixture system as the condensed water can help overcome the kinetic barrier, leading to crystallization (Gupta et al., 2015). All types of MBTCA particles maintained the crystal phase until RH = 95%. Among 100 particles, type 1-3 particles accounted for approximately 25%, 5%, and 70%, respectively. Based on the experimental results, MBTCA droplets have DRH > 95% and ERH = 30–58%. This is the first study reporting the hygroscopic properties of MBTCA. A previous study showed that MBTCA was not hydrated significantly in the ambient atmosphere (Kildgaard et al., 2018), implying that the MBTCA solids stay in the air once they effloresced, based on our results.

3.2 Hygroscopic behavior of mono-/di-/tri-sodium MBTCA salt aerosols

The hygroscopicity and Raman spectra of mono-/di-/tri-sodium MBTCA salt aerosols (hereafter, denoted as NaH_2M, Na_2HM, and Na_3M, respectively) were studied to examine the hygroscopic behavior and estimate the chemical reactivity of MBTCA with NaCl. Figs. 3(a)-(c) show the 2-D projected area ratio plot of aerosol particles generated from 0.3 M NaH_2M, Na_2HM, and Na_3M aqueous solutions as a

https://doi.org/10.5194/acp-2020-428
Preprint. Discussion started: 29 May 2020


Atmospheric Chemistry and Physics Discussions

277 function of the RH together with the corresponding optical images and Raman spectra recorded at specific
278 RHs. As shown in Figs. 3(a) and (b), NaH_2M and Na_2HM aerosols shrank and grew continuously without
279 a phase transition during the dehydration and humidification processes, respectively, which is also
280 reflected in the optical images and Raman spectra, where they maintained their circular morphology only
281 with a change in size and the same Raman peak patterns and positions with small variations in the relative
282 peak intensities during the entire process. The water peak at ~3400-3500 cm^{-1} can still be observed at the
283 end of the dehydration process. Even after being kept in a desiccator for two months, NaH_2M and Na_2HM
284 particles still showed the same shapes and Raman spectra with those at RHs = 3.4% and 2.8%,
285 respectively. These results indicate the non-crystallizable properties and supersaturated amorphous phase
286 state of the particles. The Na_3M particles behaved differently as they did not crystallize during the
287 dehydration process. On the other hand, the aerosols exhibited efflorescence at RH = 46.8% during the
288 humidification process (Fig. 3(c)), deliquesced to become a droplet at RH = 53.1%, and grew continuously
289 after that with increasing RH. The Raman spectra of the Na_3M particles in Fig. 3(c) showed that the peak
290 at 1420-1460 cm^{-1} became two sharp peaks when the particles effloresced, and the OH peak at 3400 cm^{-1}
291 indicates that Na_3M particles possibly exist in the hydrated form. The Na_3M particles behaved
292 analogously to type 3 MBTCA particles, which might be due to their similar structures when all three
293 COOH in MBTCA were replaced with COONa upon the reaction between MBTCA with NaOH. Based
294 on the top Raman spectra of aqueous MBTCA, NaH_2M, Na_2HM, and Na_3M aerosols in Figs. 2 and 3, the
295 ratios of the CH peak at ~1460 cm^{-1} to the C=O peak at ~1720 cm^{-1} (from COOH) and to the C=O peak
296 at ~1420 cm^{-1} (from COO^-) increased and decreased in the order of MBTCA, NaH_2M, Na_2HM, and Na_3M
297 because of their reduced and elevated levels of COOH and COO^-, respectively.
298
299 **3.3 Hygroscopic behavior of MBTCA-NaCl mixture aerosols**
300 Aerosols were generated by the nebulization of MBTCA-NaCl mixture solutions of molar mixing
301 ratios of MBTCA:NaCl = 1:1, 1:2, 1:3, and 2:1 and deposited on Si wafer substrates, while maintaining
302 the entire hygroscopic measurement system at RH > 90%. The hygroscopic behavior was investigated for
303 ~10 individual aerosols of each mixing ratio, which are discussed in the following sections.
304

https://doi.org/10.5194/acp-2020-428
Preprint. Discussion started: 29 May 2020


Atmospheric Chemistry and Physics Discussions

3.3.1 Aerosols generated from solutions of MBTCA:NaCl = 1:1 and 2:1

Fig. 4 presents the hygroscopic curves of representative aerosols nebulized from solutions of MBTCA:NaCl mixtures at different molar ratios (1:1 and 2:1) along with the corresponding optical images and Raman spectra at specific RHs. During the dehydration process, the circular liquid droplets decreased in size gradually without any noticeable phase change. The Raman peak patterns were maintained only with the C=O peak at 1721 cm^{-1} (from COOH) shifting mildly rightwards, the water peak at 3466 cm^{-1} becoming undetectable, and the relative peak intensities at ~1411, 1457, and 1721 cm^{-1} varied when the RH was as low as 1.2%, indicating that the liquid droplets formed amorphous solids. The peak at 1680 cm^{-1} on the Raman spectra of MBTCA:NaCl = 2:1 at RH = 1.2% suggested that the amorphous structure of the remaining MBTCA had been retained. Both MBTCA and NaCl have their DRHs and ERHs. Therefore, a step-wise efflorescence would happen if it is assumed that the mixture aerosols are an MBTCA-NaCl binary system, i.e., a component of the aqueous droplets precipitates first at their specific ERHs depending on their mixing ratios, and the second crystallization from the remnant eutonic solution occurs at their mutual ERH (MERH) with further decreases in RH, which is independent of the mixing ratios, generally forming a heterogeneous, core-shell crystal structure owing to the two-stage crystallization process (Ge et al., 1996; Gupta et al., 2015). However, the particles of MBTCA:NaCl = 1:1 and 2:1 mixing ratios did not follow the step-wise transitions in the present study, revealing that the aerosols do not belong to the MBTCA-NaCl binary system and the chemical compositions evolved during the hygroscopic experiment due to the reaction between MBTCA and NaCl, which will be discussed later.

During the humidification process, aerosol particles of two mixing ratios grew continuously when the RH was increased from 1.2% to 90% with C=O peak (from COOH) shifting back to ~1721 cm^{-1} and the water peak becoming significant, as shown in Fig. 4. Several small crystal-like spots, which are marked by a dotted circle on the inset optical image beside the hygroscopic curve in Fig. 4(a), appeared in the particles with the mixing ratio of MBTCA:NaCl = 1:1 when the RH was increased to 67.2% and dissolved completely at RH = 71.2%. As the Raman spectra did not show any signals of the crystallized organics and RH = 71.2% is close to the DRH of pure NaCl (75(±0.5)%), the crystal-like moieties should result from the effloresced NaCl. The more noticeable water peak in the Raman spectrum taken at RH = 71.2% than that at RH = 67.2% also supports that the NaCl dissolved at RH = 71.2% as NaCl is quite hygroscopic

https://doi.org/10.5194/acp-2020-428
Preprint. Discussion started: 29 May 2020


Atmospheric Chemistry and Physics Discussions

(Li et al., 2017). No phase transition of NaCl was detected during the dehydration process, probably because the supersaturated organic moiety inhibited the crystallization of NaCl. The observation of effloresced particles during the humidification process might be caused by the structural re-arrangement of the amorphous particles upon the slow and continuous absorption of moisture with increasing RH (Mikhailov et al., 2009), leading to less restriction to NaCl crystallization. Indeed, organics in organic-inorganic mixture aerosols were reported to be a minor disturbance to the DRH of inorganic salts; in contrast, they may markedly decrease the ERH of inorganic salts depending on the organic type (Parsons et al., 2004).

3.3.2 Aerosols generated from solutions of MBTCA:NaCl = 1:2 and 1:3

Fig. 5 shows the hygroscopic curves of aerosol particles nebulized from solutions of MBTCA:NaCl with molar mixing ratios of 1:2 and 1:3, together with the corresponding optical images and Raman spectra at the transition RHs. During the dehydration process, droplets from the solutions of MBTCA:NaCl = 1:2 and 1:3 decreased gradually in size owing to water evaporation until a single-stage transition was observed at RHs = 47.2-46.5% and 46.7-45.8%, respectively, where the particle shape became less circular in the optical images. At this point, the following were observed in the Raman spectra: the water peak at 3455 cm^{-1} disappeared; the C=O peak at ~1722/1720 cm^{-1} (from COOH) shifted slightly rightwards; the relative peak intensities at 1417/1416, 1461, and 1722/1720 cm^{-1} varied. With the further decreases in RH until ~6%, the particles kept their size and shape. During the humidification process, all particles of MBTCA:NaCl = 1:2 and 1:3 maintained their structure until RHs = 50% and 40%, respectively, where they experienced a size decrease due to structural re-arrangement until RH = ~70%, grew continuously to become circular at RH = ~73%, and totally deliquesced into homogeneous droplets at RHs = 73.9% and 74.5%, respectively. Particle size and water peak increased rapidly, and the C=O peak (COOH) shifted back to 1720 cm^{-1}. Upon a further increase in RH, they grew continuously by water absorption. The ERH and DRH were attributed to the NaCl moiety as the Raman spectra maintained the peak patterns during the entire process, and the organic components condensed onto the NaCl crystal core almost simultaneously as an amorphous shell when efflorescence occurred, which is also indicated by the optical images. Before the complete deliquescence of the NaCl crystal core, the water peak at ~3455 cm^{-}

https://doi.org/10.5194/acp-2020-428
Preprint. Discussion started: 29 May 2020


Atmospheric Chemistry and Physics Discussions

[1] in the Raman spectra and the optical images at RH = 72.4% and 73.8% of the particles from the MBTCA:NaCl = 1:2 and 1:3 solutions show that the organic shell was in the liquid phase, meaning that the mixture particles were in a solid-liquid equilibrium state (Sun et al., 2018).

All the particles from MBTCA:NaCl = 1:2 and 1:3 solutions showed hysteresis curves with ERHs in the range of 46.7-45.2% and 47.2-45.6%, respectively, and DRHs = 73.9(±0.3)% and 74.5(±0.3)%, respectively.

3.3.3 Chemical reactivity of aerosols generated from MBTCA−NaCl mixture solutions

The first Raman spectra of the aerosols generated from MBTCA-NaCl mixture solutions in Figs. 4 and 5 were obtained before the dehydration process, which are comparable to that of pure MBTCA droplet particle in Fig. 2 except for a much stronger free water peak at 3450-3470 cm^{-1} due to the presence of a more hygroscopic NaCl moiety. This suggests that upon nebulization from the solutions, the mixture droplets were mostly the MBTCA-NaCl binary system. The Raman spectra obtained at the beginning of the dehydration process and the end of the humidification process revealed increased and decreased ratios of the CH peak at ~1460 cm^{-1} to the C=O peaks at ~1720 cm^{-1} (from COOH) and ~1412 cm^{-1} (from COO^-), respectively, which implies that the reaction between MBTCA and NaCl occurred during the hygroscopic experiment, leading to the decreased and increased levels of the COOH and COO^- moieties, respectively. Fig. 6(a) presents the Raman spectra of particles generated from MBTCA:NaCl = 1:1, 1:2, and 1:3 solutions together with that of NaH_2M particles obtained at the end of humidification by normalizing to the CH peak at 1458 cm^{-1}. The C=O peak intensities at 1720 cm^{-1} (from COOH) and 1412 cm^{-1} (from COO^-) of the particles generated from the mixture solutions were higher and lower, respectively, than those of the NaH_2M particle, suggesting that the aerosols generated from the MBTCA-NaCl solutions produced only NaH_2M as the reaction product between MBTCA and NaCl, regardless of the mixing ratios. The droplet particles after the humidification process were present as an MBTCA-NaCl-NaH_2M ternary system with varying compositions. As the first acid dissociation constant of MBTCA (pKa_1 = 3.59) is more than 1 and 3 orders of magnitude larger than the second (pKa_2 = 4.85) and third (pKa_3 = 6.79), respectively, H_2M^- is more abundant than HM^{2-} and M^{3-}. The chemical reaction between NaCl and MBTCA would occur in the aqueous phase as follows:

https://doi.org/10.5194/acp-2020-428
Preprint. Discussion started: 29 May 2020


Atmospheric Chemistry and Physics Discussions

389

390 MBTCA(aq) + H_2M^-(aq) + H^+(aq)+ Na^+(aq) + Cl^-(aq) → MBTCA(aq) + H_2M^-(aq) + Na^+(aq) +
391 Cl^-(aq) + HCl(g)↑ → NaH_2M (+ MBTCA, amorphous) + NaCl(s) after the efflorescence

392

393 The NaH_2M particles may exist as amorphous particles, as described before in section 3.2. Raman spectra
394 of standard aerosols generated from solutions of MBTCA:NaH_2M = 0:1, 1:1, and 1:0 were obtained at
395 different RHs to estimate the chemical reactivity of the aerosol particles generated from the MBTCA-
396 NaCl mixture solutions, which were used as a calibration curve to help determine the relative MBTCA
397 and NaH_2M contents in the aerosols at specific RHs. The estimation of the chemical reactivity between
398 malonic acid and NaCl performed in the similar way was reported in a previous study (Li et al., 2017).
399 The Raman spectra of MBTCA, NaH_2M, and mixture aerosols of MBTCA:NaH_2M = 1:1 obtained at RH
400 = 90% and normalized to the CH_3 peak at 1460 cm^{-1} showed that the intensity ratio of the two peaks at
401 1460 cm^{-1} (CH_3) and ~1720 cm^{-1} (C=O from COOH) (i.e., I_{1460}/I_{1720}) increased with increasing NaH_2M
402 level because of the decreased COOH content, as shown in Fig. 6(b). The ratio, I_{1460}/I_{1720}, for each
403 standard aerosol exhibited good linearity as a function of RH, as shown in Fig. 7(a), where the mean
404 values obtained from 10 aerosols of each standard aerosol sample are plotted with error-bars. The Raman
405 intensity ratios of the standard aerosols increased with decreasing RH because the C=O stretching
406 vibrations of the free COOH group in the aqueous phase and the intramolecular hydrogen-bonded COOH
407 group in the supersaturated phase become weaker and stronger (Bertran et al., 2010), respectively, with
408 decreasing RH during the dehydration process.

409 The dependency of the I_{1460}/I_{1720} ratios on RH can be used to estimate the MBTCA and NaH_2M
410 (monosodium MBTCA salt) contents in the NaCl-MBTCA aerosols at specific RHs based on the
411 calibration curve and to calculate the further reactivity. The chemical reactivity of the mixtures is
412 represented as the degree of the reaction, which is defined as the ratio of consumed to the original amount
413 of the limiting reactant. For example, for aerosols from solutions of MBTCA:NaCl = 2:1 and 1:2, NaCl
414 and MBTCA are the limiting reactants, respectively. Fig. 7(b) shows the degree of the reaction of aerosols
415 generated from solutions of each mixing ratio, where the mean degree of reaction has ~1.5-4% deviations
416 owing to statistical variations in the Raman peak intensities caused by the baseline correction procedure

https://doi.org/10.5194/acp-2020-428
Preprint. Discussion started: 29 May 2020


Atmospheric Chemistry and Physics Discussions

and the uncertainties involved in the calibration measurements. The reactivity was estimated at five stages during one cycle hygroscopic experiment.

Stage 1; At the beginning of the hygroscopic experiment, no reaction occurred for all the mixed droplets based on their Raman spectra, i.e., the degree of the reaction is 0.

Stage 2; As the RH decreased during the dehydration process, the reaction continued in the aqueous aerosols until efflorescence of the droplets with mixing ratios of MBTCA:NaCl = 1:2 and 1:3 had occurred, and until the water content of the aerosols with mixing ratios of MBTCA:NaCl = 1:1 and 2:1 became insignificant. The degrees of the reaction of aerosols with mixing ratios of 1:1, 1:2, and 1:3 were approximately 30%, whereas that of 2:1 approached 85%.

Stage 3; The reaction of aerosols generated from the solution of mixing ratio of MBTCA:NaCl = 2:1 was complete at the end of the dehydration process, indicating the total consumption of NaCl and the formation of an MBTCA:NaH_2M = 1:1 mixture aerosol. The Raman spectra of the aerosols with mixing ratios of MBTCA:NaCl = 1:1, 1:2, and 1:3 at the end of the dehydration process were unsuitable for the reactivity estimation mostly due to their heterogeneous structure in the presence of a NaCl core.

Stages 4 and 5; The reaction proceeded after deliquescence when the free H^+ and Cl^- became available again for aerosols with mixing ratios of MBTCA:NaCl = 1:1, 1:2, and 1:3, and a small increase in the degree of reaction (~5%) was observed at the end of humidification for these mixture droplets.

Most of the reactions occurred in the aqueous phase during the dehydration process with considerable amounts of aqueous H^+ from MBTCA and Cl^- from NaCl available for HCl liberation. During the entire experiment, the reactivity followed the sequence of MBTCA:NaCl = 2:1 > 1:3 > 1:2 > 1:1, where the reactivity appeared to be enhanced when either of the reactants is enriched. On the other hand, the reaction

https://doi.org/10.5194/acp-2020-428
Preprint. Discussion started: 29 May 2020


Atmospheric Chemistry and Physics Discussions

was complete only when aqueous H^+ was sufficiently available, i.e., the reaction depended mostly on the triacid level. The real-time aerosol mixture components based on the reactivity estimation of each mixing ratio at specific RHs are shown on the hygroscopic curves in Figs. 4 and 5.

The morphology and elemental distribution of effloresced MBTCA-NaCl particles were examined by SEM/EDX. Figure 8(a) shows the secondary electron images (SEIs) of the exemplar particles of each mixing ratio. The elemental X-ray maps for MBTCA:NaCl = 1:1 and 1:2 particles suggest that the NaCl solid moiety (represented by Na and Cl X-ray maps) crystallized homogeneously at small spots inside the organic moiety. For MBTCA:NaCl = 1:3 particles with a significant amount of NaCl, the NaCl solid existed as a core surrounded by the organic moiety. The organic mixture of MBTCA and NaH_2M (represented by C and Na) condensed onto the NaCl core almost simultaneously when efflorescence occurred, while maintaining a relatively circular morphology, even after being inserted into the vacuum SEM chamber, which also indicates the low crystallization tendency of the organic moiety. The different shapes of organic shell-inorganic core structures depending on the organic mass fraction and RH are reported elsewhere (Karadima et al., 2019). The homogeneous structure of C and Na and the absence of Cl for particles with mixing ratios of MBTCA:NaCl = 2:1, as shown in the corresponding SEIs and X-ray spectrum in Figs. 8(a) and (b), confirmed that the reaction was complete at the end of the dehydration process. The reaction between MBTCA and NaCl and the changes in the microstructures after the reaction are expected to have some atmospheric implications since they may have enhanced ability to facilitate further heterogeneous reactions in the atmosphere because of their low crystallization property. Na (from both NaH_2M and NaCl) and Cl (from NaCl) levels were used to estimate the degrees of reaction for the MBTCA:NaCl = 1:1, 1:2, 1:3, and 2:1 systems, which were estimated to be ~25%, ~30%, ~37%, and 100%, respectively, with well matching to those from the Raman analysis by 5-8% differences.

3.4 Hygroscopic behavior of pure MBTCA and MBTCA−NaCl mixture particles in the levitation system

The data acquired from the levitation system for contactless experiments on particles of ~80-100 μm were used to compare with those obtained for aerosols on the Si wafer in the see-through impactor.

https://doi.org/10.5194/acp-2020-428
Preprint. Discussion started: 29 May 2020


Atmospheric Chemistry and Physics Discussions

Two types of hygroscopic behavior of pure MBTCA particles were observed, corresponding closely to types 1 and 3 aerosol particles in the see-through impactor system. In addition, the ERH was ~49-54%, confirming that once overcome the kinetic barrier and effloresce into solids, the MBTCA particles no longer capture water significantly. The Raman spectra and optical images are not shown separately.

The droplets composed of MBTCA:NaCl = 1:1, 1:2, and 1:3 mixing ratios were introduced into the levitator and dried rapidly at RH = ~10% within 15 minutes (first rapid dehydration, i.e., the quenching process), and humidified progressively to RH = 80%. Once RH = 80%, the particles dehydrated gradually until RH = ~10% (second dehydration). The Raman spectra and optical images are shown in Fig. S2. After the first rapid dehydration of the particles, the existence of peaks at 1660 and 1720 cm^{-1} was observed for all the mixtures, and the relative intensity of the peak at ~1720 cm^{-1} increased with increasing NaCl content, suggesting the formation of the mixture of solid MBTCA and amorphous moiety either from MBTCA or NaH_2M. During the humidification process, the Raman peak at 1720 cm^{-1} and the particle size grew continuously with increasing RH. Transitions were observed at RH = ~71%, ~74.5%, and ~75% for MBTCA:NaCl = 1:1, 1:2, and 1:3 mixture particles, respectively, with the water peak at ~3500 cm^{-1} becoming significant for the three compositions. The observed transition points were attributed to the deliquescence of NaCl within the particle with the MBTCA moiety partially remaining as a solid phase, and the elevated NaCl content strongly enhanced the ability of the particles to uptake water. The peak related to the solid portion at 1655 cm^{-1} disappeared only for the MBTCA:NaCl = 1:3 mixture particles at the end of humidification, suggesting that the particle had transformed completely into a droplet. During the second dehydration process, the particles showed the entire release of water, as illustrated by the disappearance of the peak at 3500 cm^{-1} at RH = ~50%, i.e., the ERH, for all the mixtures while maintaining the peak patterns and positions until the lowest RH. The Raman spectra recorded at the end of dehydration revealed both solid and amorphous phases for the MBTCA:NaCl = 1:1 and 1:2 mixtures due to the existence of the peaks at 1660 and 1720 cm^{-1}. In contrast, only the 1720 cm^{-1} associated with the amorphous composition was observed for the MBTCA:NaCl = 1:3 mixture, suggesting that the reaction between MBTCA and NaCl was facilitated extensively by the increased NaCl concentration while absorbing sufficient moisture. The conspicuous DRHs and ERHs of all the mixtures in the levitation system demonstrated a smaller degree of reaction between MBTCA and NaCl compared

https://doi.org/10.5194/acp-2020-428
Preprint. Discussion started: 29 May 2020


Atmospheric Chemistry and Physics Discussions

to those obtained in the see-through impactor, which might be caused by the relatively closed atmosphere in the levitator, i.e., less release of HCl, and the starting point of the hygroscopic cycle, i.e., the quenching process resulting in partially effloresced MBTCA before the humidification process.

4. Conclusions and atmospheric implication

The hygroscopic behavior, physical states, and chemical reactivity of pure MBTCA particles, mono-/di-/tri-sodium MBTCA salt particles, and MBTCA-NaCl particles of different mixing ratios were examined by in situ RMS assembled with a see-through impactor as the starting point with dehydration. The DRHs and ERHs of the laboratory-generated particles in the micrometer size range at room temperature were determined by monitoring the change in the particle area in the 2-D optical images and the corresponding Raman spectra at transition points with RH variation of ~1-95%. Pure MBTCA showed three types of hygroscopic behaviors in that types 1 and 2 particles effloresced suddenly and gradually, respectively, at ERH = 30-58% during the dehydration process, whereas type 3 particles crystallized during the humidification process at RH = ~37%, not during the dehydration process because of a kinetic barrier to nucleation with limited condensed water. Subsequently, all particles maintained their crystal structure until RH = 95%. The mono- and di-sodium MBTCA salt aerosols did not show a clear efflorescence RH (ERH) and deliquescence RH (DRH) during the dehydration and humidification processes, respectively. In contrast, the tri-sodium MBTCA showed ERH = ~44.4-46.8% (during humidification) and DRH = ~53.1%. The MBTCA-NaCl droplets with molar mixing ratios of MBTCA:NaCl = 1:1 and 2:1 showed no distinct DRH and ERH because of the partial and complete reactions with NaCl, respectively, whereas those with ratios of MBTCA:NaCl =1:2 and 1:3 experienced single-stage efflorescence and deliquescence governed by the excess NaCl. Only monosodium MBTCA (NaH_2M) could be formed as a result of the reaction between NaCl and MBTCA regardless of the mixing ratios, mostly during the dehydration process within the timescale of one to two hours according to Raman analysis, indicating that the MBTCA-NaCl mixture systems are in an MBTCA-NaH_2M-NaCl ternary system except when NaCl has reacted completely in the mixture aerosols of MBTCA:NaCl = 2:1 ratio. The MBTCA-NaH_2M existed as amorphous solids, even when the excess crystalline NaCl acted as a heterogeneous nucleation core, which was also confirmed by X-ray mapping. The reaction occurred more

https://doi.org/10.5194/acp-2020-428
Preprint. Discussion started: 29 May 2020


Atmospheric Chemistry and Physics Discussions

528 rapidly with a more elevated concentration of either MBTCA or NaCl, and the controlling factor for the
529 reactivity of the mixtures depended mostly on the availability of H^+ dissociated from the MBTCA
530 tricarboxylic acid. The hygroscopic experiments for pure MBTCA and MBTCA-NaCl mixture particles
531 were also performed in a levitation system with the starting point from humidification after the quenching
532 process and the RH variation of ~10 to 80%. The results acquired from the levitation system are consistent
533 with those obtained from the see-through impactor, only with less reaction between MBTCA and NaCl
534 resulting from the airtight atmosphere inside the levitator and the partial solidification of MBTCA after
535 the quenching process. In addition, the elevated NaCl moiety can eventually transform the solidified
536 MBTCA into droplets through reactions when absorbing adequate moisture.
537 These observations are expected to have important atmospheric implications in that they may help to
538 better understand the complexity of real ambient SOA and inorganic mixture particles. In this study, the
539 hygroscopicity of MBTCA was altered significantly when mixed with NaCl due to the reaction, so that
540 they are more likely to contribute to further gas-particle interactions. The amorphous phase state may
541 influence the uptake of gaseous photo-oxidants as well as the chemical transformation and aging of
542 atmospheric aerosols (Mikhailov et al., 2009). The observed aqueous shell with the solid core upon the
543 humidification of the mixture particles with mixing ratios of MBTCA:NaCl = 1:2 and 1:3 before the total
544 dissolution of NaCl can scatter solar radiation more efficiently (Adachi et al., 2011; Sun et al., 2018). The
545 aerosol liquid water can promote heterogeneous aqueous-phase chemical processes, resulting in the facile
546 formation of secondary aerosols (Cheng et al., 2016; Li et al., 2019). Recently, heterogeneous reactions
547 in aerosol water were reported to be a significant mechanism for haze formation in North China (Sun et
548 al., 2018). Overall, the hygroscopic curve, Raman signatures, and X-ray maps of the effloresced particles
549 provided clear features of the hygroscopic behavior and chemical reactivity of the MBTCA-NaCl mixture
550 system covered in this study. These results are expected to provide insights into the physicochemical
551 characteristics and atmospheric chemistry of highly oxidized SOAs mixed with inorganic particles.
552
553 *Data availability.* The data used in this study are available upon request; please contact Chul-Un Ro
554 (curo@inha.ac.kr).
555

https://doi.org/10.5194/acp-2020-428
Preprint. Discussion started: 29 May 2020


Atmospheric Chemistry and Physics Discussions

556 *Author contributions.* LW, CB, SS, and CR designed the experiment. LW, CB, and SS carried out the
557 measurements and/or analyzed the data. LW, CB, SS, PF, EP, EV, YS and CR contributed discussion of
558 the data. LW, SS, and CR drafted the paper.
559
560 *Competing interests.* The authors declare that they have no conflict of interest.
561
562 *Acknowledgments.* This study was supported by Basic Science Research Programs through the National
563 Research Foundation of Korea (NRF) funded by the Ministry of Education, Science, and Technology
564 (NRF-2018R1A2A1A05023254). Authors thank the Region Nouvelle Aquitaine for the financial support
565 of the SPECAERO project. This work was performed through international and collaborative programs
566 supported by PHC STAR n° 38815XE and visiting scholars program from IDEX of the University of
567 Bordeaux.
568
569 **References**

570 Adachi, K., Freney, E. J., and Buseck, P. R.: Shapes of internally mixed hygroscopic aerosol particles
571 after deliquescence, and their effect on light scattering, Geophysical Research Letters, 38, n/a-
572 n/a, 10.1029/2011gl047540, 2011.
573 Ahn, K.-H., Kim, S.-M., Jung, H.-J., Lee, M.-J., Eom, H.-J., Maskey, S., and Ro, C.-U.: Combined use
574 of optical and electron microscopic techniques for the measurement of hygroscopic property,
575 chemical composition, and morphology of individual aerosol particles, Analytical chemistry, 82,
576 7999-8009, 2010.
577 Aljawhary, D., Zhao, R., Lee, A. K., Wang, C., and Abbatt, J. P.: Kinetics, Mechanism, and Secondary
578 Organic Aerosol Yield of Aqueous Phase Photo-oxidation of alpha-Pinene Oxidation Products, J
579 Phys Chem A, 120, 1395-1407, 10.1021/acs.jpca.5b06237, 2016.
580 An, P., Yuan, C.-Q., Liu, X.-H., Xiao, D.-B., and Luo, Z.-X.: Vibrational spectroscopic identification of
581 isoprene, pinenes and their mixture, Chinese Chemical Letters, 27, 527-534,
582 10.1016/j.cclet.2016.01.036, 2016.
583 Bateman, A. P., Bertram, A. K., and Martin, S. T.: Hygroscopic influence on the semisolid-to-liquid
584 transition of secondary organic materials, J Phys Chem A, 119, 4386-4395, 10.1021/jp508521c,
585 2015a.
586 Bateman, A. P., Gong, Z., Liu, P., Sato, B., Cirino, G., Zhang, Y., Artaxo, P., Bertram, A. K., Manzi, A.
587 O., Rizzo, L. V., Souza, R. A. F., Zaveri, R. A., and Martin, S. T.: Sub-micrometre particulate
588 matter is primarily in liquid form over Amazon rainforest, Nature Geoscience, 9, 34-37,
589 10.1038/ngeo2599, 2015b.

https://doi.org/10.5194/acp-2020-428
Preprint. Discussion started: 29 May 2020


Atmospheric Chemistry and Physics Discussions

590 Berkemeier, T., Shiraiwa, M., Pöschl, U., and Koop, T.: Competition between water uptake and ice
591 nucleation by glassy organic aerosol particles, Atmospheric Chemistry and Physics, 14, 12513-
592 12531, 10.5194/acp-14-12513-2014, 2014.
593 Bernard, F., Ciuraru, R., Boreave, A., and George, C.: Photosensitized Formation of Secondary Organic
594 Aerosols above the Air/Water Interface, Environ Sci Technol, 50, 8678-8686,
595 10.1021/acs.est.6b03520, 2016.
596 Bertran, O., Armelin, E., Estrany, F., Gomes, A., Torras, J., and Alemán, C.: Poly (2-thiophen-3-yl-
597 malonic acid), a polythiophene with two carboxylic acids per repeating unit, The Journal of
598 Physical Chemistry B, 114, 6281-6290, 2010.
599 Cheng, Y., Zheng, G., Wei, C., Mu, Q., Zheng, B., Wang, Z., Gao, M., Zhang, Q., He, K., and
600 Carmichael, G.: Reactive nitrogen chemistry in aerosol water as a source of sulfate during haze
601 events in China, Science Advances, 2, e1601530, 2016.
602 Chu, B., Wang, K., Takekawa, H., Li, J., Zhou, W., Jiang, J., Ma, Q., He, H., and Hao, J.:
603 Hygroscopicity of particles generated from photooxidation of α-pinene under different oxidation
604 conditions in the presence of sulfate seed aerosols, Journal of Environmental Sciences, 26, 129-
605 139, 10.1016/s1001-0742(13)60402-7, 2014.
606 Clegg, S. L., Seinfeld, J. H., and Edney, E. O.: Thermodynamic modelling of aqueous aerosols
607 containing electrolytes and dissolved organic compounds. II. An extended Zdanovskii–Stokes–
608 Robinson approach, Journal of aerosol science, 34, 667-690, 2003.
609 Cui, T., Green, H. S., Selleck, P. W., Zhang, Z., O'Brien, R. E., Gold, A., Keywood, M., Kroll, J. H.,
610 and Surratt, J. D.: Chemical Characterization of Isoprene- and Monoterpene-Derived Secondary
611 Organic Aerosol Tracers in Remote Marine Aerosols over a Quarter Century, ACS Earth and
612 Space Chemistry, 3, 935-946, 10.1021/acsearthspacechem.9b00061, 2019.
613 Dette, H. P., Qi, M., Schroder, D. C., Godt, A., and Koop, T.: Glass-forming properties of 3-
614 methylbutane-1,2,3-tricarboxylic acid and its mixtures with water and pinonic acid, J Phys
615 Chem A, 118, 7024-7033, 10.1021/jp505910w, 2014.
616 Ding, X., Wang, X.-M., Gao, B., Fu, X.-X., He, Q.-F., Zhao, X.-Y., Yu, J.-Z., and Zheng, M.: Tracer-
617 based estimation of secondary organic carbon in the Pearl River Delta, south China, Journal of
618 Geophysical Research: Atmospheres, 117, n/a-n/a, 10.1029/2011jd016596, 2012.
619 Donahue, N. M., Henry, K. M., Mentel, T. F., Kiendler-Scharr, A., Spindler, C., Bohn, B., Brauers, T.,
620 Dorn, H. P., Fuchs, H., Tillmann, R., Wahner, A., Saathoff, H., Naumann, K. H., Mohler, O.,
621 Leisner, T., Muller, L., Reinnig, M. C., Hoffmann, T., Salo, K., Hallquist, M., Frosch, M., Bilde,
622 M., Tritscher, T., Barmet, P., Praplan, A. P., DeCarlo, P. F., Dommen, J., Prevot, A. S., and
623 Baltensperger, U.: Aging of biogenic secondary organic aerosol via gas-phase OH radical
624 reactions, Proc Natl Acad Sci U S A, 109, 13503-13508, 10.1073/pnas.1115186109, 2012.
625 Donahue, N. M., Ortega, I. K., Chuang, W., Riipinen, I., Riccobono, F., Schobesberger, S., Dommen, J.,
626 Baltensperger, U., Kulmala, M., Worsnop, D. R., and Vehkamaki, H.: How do organic vapors
627 contribute to new-particle formation?, Faraday Discussions, 165, 10.1039/c3fd00046j, 2013.
628 Dunne, E. M., Gordon, H., Kurten, A., Almeida, J., Duplissy, J., Williamson, C., Ortega, I. K., Pringle,
629 K. J., Adamov, A., Baltensperger, U., Barmet, P., Benduhn, F., Bianchi, F., Breitenlechner, M.,
630 Clarke, A., Curtius, J., Dommen, J., Donahue, N. M., Ehrhart, S., Flagan, R. C., Franchin, A.,
631 Guida, R., Hakala, J., Hansel, A., Heinritzi, M., Jokinen, T., Kangasluoma, J., Kirkby, J.,

Kulmala, M., Kupc, A., Lawler, M. J., Lehtipalo, K., Makhmutov, V., Mann, G., Mathot, S., Merikanto, J., Miettinen, P., Nenes, A., Onnela, A., Rap, A., Reddington, C. L., Riccobono, F., Richards, N. A., Rissanen, M. P., Rondo, L., Sarnela, N., Schobesberger, S., Sengupta, K., Simon, M., Sipila, M., Smith, J. N., Stozkhov, Y., Tome, A., Trostl, J., Wagner, P. E., Wimmer, D., Winkler, P. M., Worsnop, D. R., and Carslaw, K. S.: Global atmospheric particle formation from CERN CLOUD measurements, Science, 354, 1119-1124, 10.1126/science.aaf2649, 2016.

Edsall, J. T.: Raman Spectra of Amino Acids and Related Compounds IV. Ionization of Di- and Tricarboxylic Acids, The Journal of Chemical Physics, 5, 508-517, 10.1063/1.1750067, 1937.

Elm, J.: Unexpected Growth Coordinate in Large Clusters Consisting of Sulfuric Acid and C8H12O6 Tricarboxylic Acid, J Phys Chem A, 10.1021/acs.jpca.9b00428, 2019.

Enami, S., and Sakamoto, Y.: OH-Radical Oxidation of Surface-Active cis-Pinonic Acid at the Air-Water Interface, J Phys Chem A, 120, 3578-3587, 10.1021/acs.jpca.6b01261, 2016.

Eom, H. J., Gupta, D., Li, X., Jung, H. J., Kim, H., and Ro, C. U.: Influence of collecting substrates on the characterization of hygroscopic properties of inorganic aerosol particles, Anal Chem, 86, 2648-2656, 10.1021/ac4042075, 2014.

Freedman, M. A.: Phase separation in organic aerosol, Chemical Society Reviews, 46, 7694-7705, 2017.

Fu, P., Kawamura, K., Chen, J., and Barrie, L. A.: Isoprene, monoterpene, and sesquiterpene oxidation products in the high Arctic aerosols during late winter to early summer, Environmental Science & Technology, 43, 4022-4028, 2009.

Fu, P. Q., Kawamura, K., Cheng, Y. F., Hatakeyama, S., Takami, A., Li, H., and Wang, W.: Aircraft measurements of polar organic tracer compounds in tropospheric particles (PM₁₀) over central China, Atmospheric Chemistry and Physics, 14, 4185-4199, 10.5194/acp-14-4185-2014, 2014.

Ge, Z., Wexler, A. S., and Johnston, M. V.: Multicomponent aerosol crystallization, Journal of Colloid and Interface Science, 183, 68-77, 1996.

Gibson, E. R., Hudson, P. K., and Grassian, V. H.: Physicochemical properties of nitrate aerosols: Implications for the atmosphere, The Journal of Physical Chemistry A, 110, 11785-11799, 2006.

Gómez-González, Y., Wang, W., Vermeylen, R., Chi, X., Neirynck, J., Janssens, I. A., Maenhaut, W., and Claeys, M.: Chemical characterisation of atmospheric aerosols during a 2007 summer field campaign at Brasschaat, Belgium: sources and source processes of biogenic secondary organic aerosol, Atmospheric Chemistry and Physics, 12, 125-138, 10.5194/acp-12-125-2012, 2012.

Guenther, A., Hewitt, C. N., Erickson, D., Fall, R., Geron, C., Graedel, T., Harley, P., Klinger, L., Lerdau, M., and McKay, W.: A global model of natural volatile organic compound emissions, Journal of Geophysical Research: Atmospheres, 100, 8873-8892, 1995.

Gupta, D., Eom, H. J., Cho, H. R., and Ro, C. U.: Hygroscopic behavior of NaCl–MgCl₂ mixture particles as nascent sea-spray aerosol surrogates and observation of efflorescence during humidification, Atmospheric Chemistry and Physics, 15, 11273-11290, 10.5194/acp-15-11273-2015, 2015.

Gysel, M., Weingartner, E., and Baltensperger, U.: Hygroscopicity of aerosol particles at low temperatures. 2. Theoretical and experimental hygroscopic properties of laboratory generated aerosols, Environmental science & technology, 36, 63-68, 2002.

https://doi.org/10.5194/acp-2020-428
Preprint. Discussion started: 29 May 2020


Atmospheric Chemistry and Physics Discussions

674 Hallquist, M., Wenger, J. C., Baltensperger, U., Rudich, Y., Simpson, D., Claeys, M., Dommen, J.,
675 Donahue, N., George, C., and Goldstein, A.: The formation, properties and impact of secondary
676 organic aerosol: current and emerging issues, Atmospheric chemistry and physics, 9, 5155-5236,
677 2009.
678 Harris, D. C.: Exploring chemical analysis, Macmillan, 2012.
679 Haywood, J., and Boucher, O.: Estimates of the direct and indirect radiative forcing due to tropospheric
680 aerosols: A review, Reviews of geophysics, 38, 513-543, 2000.
681 Hoffman, R. C., Laskin, A., and Finlayson-Pitts, B. J.: Sodium nitrate particles: physical and chemical
682 properties during hydration and dehydration, and implications for aged sea salt aerosols, Journal
683 of Aerosol Science, 35, 869-887, 10.1016/j.jaerosci.2004.02.003, 2004.
684 Holopainen, J. K., Kivimaenpaa, M., and Nizkorodov, S. A.: Plant-derived Secondary Organic Material
685 in the Air and Ecosystems, Trends Plant Sci, 22, 744-753, 10.1016/j.tplants.2017.07.004, 2017.
686 Hong, Z., Zhang, H., Zhang, Y., Xu, L., Liu, T., Xiao, H., Hong, Y., Chen, J., Li, M., Deng, J., Wu, X.,
687 Hu, B., and Chen, X.: Secondary organic aerosol of PM2.5 in a mountainous forest area in
688 southeastern China: Molecular compositions and tracers implication, Sci Total Environ, 653,
689 496-503, 10.1016/j.scitotenv.2018.10.370, 2019.
690 Hu, D., Bian, Q., Li, T. W. Y., Lau, A. K. H., and Yu, J. Z.: Contributions of isoprene, monoterpenes,β-
691 caryophyllene, and toluene to secondary organic aerosols in Hong Kong during the summer of
692 2006, Journal of Geophysical Research, 113, 10.1029/2008jd010437, 2008.
693 Hu, Q. H., Xie, Z. Q., Wang, X. M., Kang, H., He, Q. F., and Zhang, P.: Secondary organic aerosols
694 over oceans via oxidation of isoprene and monoterpenes from Arctic to Antarctic, Sci Rep, 3,
695 2280, 10.1038/srep02280, 2013.
696 Jang, M., Czoschke, N. M., Lee, S., and Kamens, R. M.: Heterogeneous atmospheric aerosol production
697 by acid-catalyzed particle-phase reactions, Science, 298, 814-817, 2002.
698 Jaoui, M., Kleindienst, T., Lewandowski, M., Offenberg, J., and Edney, E.: Identification and
699 quantification of aerosol polar oxygenated compounds bearing carboxylic or hydroxyl groups. 2.
700 Organic tracer compounds from monoterpenes, Environmental science & technology, 39, 5661-
701 5673, 2005.
702 Jimenez, J. L., Canagaratna, M., Donahue, N., Prevot, A., Zhang, Q., Kroll, J. H., DeCarlo, P. F., Allan,
703 J. D., Coe, H., and Ng, N.: Evolution of organic aerosols in the atmosphere, science, 326, 1525-
704 1529, 2009.
705 Jing, B., Tong, S., Liu, Q., Li, K., Wang, W., Zhang, Y., and Ge, M.: Hygroscopic behavior of
706 multicomponent organic aerosols and their internal mixtures with ammonium sulfate,
707 Atmospheric Chemistry and Physics, 16, 4101-4118, 10.5194/acp-16-4101-2016, 2016.
708 Jing, B., Wang, Z., Tan, F., Guo, Y., Tong, S., Wang, W., Zhang, Y., and Ge, M.: Hygroscopic behavior
709 of atmospheric aerosols containing nitrate salts and water-soluble organic acids, Atmospheric
710 Chemistry and Physics, 18, 5115-5127, 10.5194/acp-18-5115-2018, 2018.
711 Kammer, J., Perraudin, E., Flaud, P. M., Lamaud, E., Bonnefond, J. M., and Villenave, E.: Observation
712 of nighttime new particle formation over the French Landes forest, Sci Total Environ, 621,
713 1084-1092, 10.1016/j.scitotenv.2017.10.118, 2018.
714 Kang, M., Fu, P., Kawamura, K., Yang, F., Zhang, H., Zang, Z., Ren, H., Ren, L., Zhao, Y., Sun, Y.,
715 and Wang, Z.: Characterization of biogenic primary and secondary organic aerosols in the

716 marine atmosphere over the East China Sea, Atmospheric Chemistry and Physics, 18, 13947-
717 13967, 10.5194/acp-18-13947-2018, 2018.
718 Karadima, K. S., Mavrantzas, V. G., and Pandis, S. N.: Insights into the morphology of multicomponent
719 organic and inorganic aerosols from molecular dynamics simulations, Atmospheric Chemistry
720 and Physics, 19, 5571-5587, 10.5194/acp-19-5571-2019, 2019.
721 Kidd, C., Perraud, V., Wingen, L. M., and Finlayson-Pitts, B. J.: Integrating phase and composition of
722 secondary organic aerosol from the ozonolysis of α-pinene, Proceedings of the National
723 Academy of Sciences, 111, 7552-7557, 2014.
724 Kildgaard, J. V., Mikkelsen, K. V., Bilde, M., and Elm, J.: Hydration of Atmospheric Molecular
725 Clusters II: Organic Acid-Water Clusters, J Phys Chem A, 122, 8549-8556,
726 10.1021/acs.jpca.8b07713, 2018.
727 Kim, H., Lee, M.-J., Jung, H.-J., Eom, H.-J., Maskey, S., Ahn, K.-H., and Ro, C.-U.: Hygroscopic
728 behavior of wet dispersed and dry deposited NaNO3 particles, Atmospheric Environment, 60,
729 68-75, 10.1016/j.atmosenv.2012.06.011, 2012.
730 Kim, H., Zhang, Q., and Heo, J.: Influence of intense secondary aerosol formation and long-range
731 transport on aerosol chemistry and properties in the Seoul Metropolitan Area during spring time:
732 results from KORUS-AQ, Atmospheric Chemistry and Physics, 18, 7149-7168, 10.5194/acp-18-
733 7149-2018, 2018.
734 Koop, T., Bookhold, J., Shiraiwa, M., and Pöschl, U.: Glass transition and phase state of organic
735 compounds: dependency on molecular properties and implications for secondary organic
736 aerosols in the atmosphere, Physical Chemistry Chemical Physics, 13, 19238-19255, 2011.
737 Kostenidou, E., Karnezi, E., Kolodziejczyk, A., Szmigielski, R., and Pandis, S. N.: Physical and
738 Chemical Properties of 3-Methyl-1,2,3-butanetricarboxylic Acid (MBTCA) Aerosol, Environ
739 Sci Technol, 52, 1150-1155, 10.1021/acs.est.7b04348, 2018.
740 Kourtchev, I., Copolovici, L., Claeys, M., and Maenhaut, W.: Characterization of atmospheric aerosols
741 at a forested site in Central Europe, Environmental science & technology, 43, 4665-4671, 2009.
742 Kroll, J. H., and Seinfeld, J. H.: Chemistry of secondary organic aerosol: Formation and evolution of
743 low-volatility organics in the atmosphere, Atmospheric Environment, 42, 3593-3624, 2008.
744 Kubátová, A., Vermeylen, R., Claeys, M., Cafmeyer, J., Maenhaut, W., Roberts, G., and Artaxo, P.:
745 Carbonaceous aerosol characterization in the Amazon basin, Brazil: novel dicarboxylic acids
746 and related compounds, Atmospheric Environment, 34, 5037-5051, 2000.
747 Kubátová, A., Vermeylen, R., Claeys, M., Cafmeyer, J., and Maenhaut, W.: Organic compounds in
748 urban aerosols from Gent, Belgium: Characterization, sources, and seasonal differences, Journal
749 of Geophysical Research: Atmospheres, 107, ICC 5-1-ICC 5-12, 10.1029/2001jd000556, 2002.
750 Lai, C., Liu, Y., Ma, J., Ma, Q., Chu, B., and He, H.: Heterogeneous Kinetics of cis-Pinonic Acid with
751 Hydroxyl Radical under Different Environmental Conditions, J Phys Chem A, 119, 6583-6593,
752 10.1021/acs.jpca.5b01321, 2015.
753 Laskin, A., Moffet, R. C., Gilles, M. K., Fast, J. D., Zaveri, R. A., Wang, B., Nigge, P., and
754 Shutthanandan, J.: Tropospheric chemistry of internally mixed sea salt and organic particles:
755 Surprising reactivity of NaCl with weak organic acids, Journal of Geophysical Research:
756 Atmospheres, 117, n/a-n/a, 10.1029/2012jd017743, 2012.

757 Lee, A. K. Y., Ling, T. Y., and Chan, C. K.: Understanding hygroscopic growth and phase
758 transformation of aerosols using single particle Raman spectroscopy in an electrodynamic
759 balance, Faraday Discuss., 137, 245-263, 10.1039/b704580h, 2008.
760 Lessmeier, J., Dette, H. P., Godt, A., and Koop, T.: Physical state of 2-methylbutane-1,2,3,4-tetraol in
761 pure and internally mixed aerosols, Atmospheric Chemistry and Physics, 18, 15841-15857,
762 10.5194/acp-18-15841-2018, 2018.
763 Li, J. J., Wang, G. H., Cao, J. J., Wang, X. M., and Zhang, R. J.: Observation of biogenic secondary
764 organic aerosols in the atmosphere of a mountain site in central China: temperature and relative
765 humidity effects, Atmospheric Chemistry and Physics, 13, 11535-11549, 10.5194/acp-13-
766 11535-2013, 2013.
767 Li, X., Gupta, D., Lee, J., Park, G., and Ro, C. U.: Real-Time Investigation of Chemical Compositions
768 and Hygroscopic Properties of Aerosols Generated from NaCl and Malonic Acid Mixture
769 Solutions Using in Situ Raman Microspectrometry, Environ Sci Technol, 51, 263-270,
770 10.1021/acs.est.6b04356, 2017.
771 Li, X., Song, S., Zhou, W., Hao, J., Worsnop, D. R., and Jiang, J.: Interactions between aerosol organic
772 components and liquid water content during haze episodes in Beijing, Atmospheric Chemistry
773 and Physics, 19, 12163-12174, 10.5194/acp-19-12163-2019, 2019.
774 Lightstone, J. M., Onasch, T. B., Imre, D., and Oatis, S.: Deliquescence, efflorescence, and water
775 activity in ammonium nitrate and mixed ammonium nitrate/succinic acid microparticles, The
776 Journal of Physical Chemistry A, 104, 9337-9346, 2000.
777 Lignell, H., Epstein, S. A., Marvin, M. R., Shemesh, D., Gerber, B., and Nizkorodov, S.: Experimental
778 and theoretical study of aqueous cis-pinonic acid photolysis, J Phys Chem A, 117, 12930-12945,
779 10.1021/jp4093018, 2013.
780 Liu, T., Zhou, L., Liu, Q., Lee, B. P., Yao, D., Lu, H., Lyu, X., Guo, H., and Chan, C. K.: Secondary
781 Organic Aerosol Formation from Urban Roadside Air in Hong Kong, Environ Sci Technol, 53,
782 3001-3009, 10.1021/acs.est.8b06587, 2019.
783 Ma, Q., Ma, J., Liu, C., Lai, C., and He, H.: Laboratory study on the hygroscopic behavior of external
784 and internal C2-C4 dicarboxylic acid-NaCl mixtures, Environ Sci Technol, 47, 10381-10388,
785 10.1021/es4023267, 2013.
786 Marsh, A., Rovelli, G., Miles, R. E. H., and Reid, J. P.: Complexity of Measuring and Representing the
787 Hygroscopicity of Mixed Component Aerosol, J Phys Chem A, 123, 1648-1660,
788 10.1021/acs.jpca.8b11623, 2019.
789 Martin, S. T.: Phase transitions of aqueous atmospheric particles, Chemical Reviews, 100, 3403-3454,
790 2000.
791 Mikhailov, E., Vlasenko, S., Martin, S., Koop, T., and Pöschl, U.: Amorphous and crystalline aerosol
792 particles interacting with water vapor: conceptual framework and experimental evidence for
793 restructuring, phase transitions and kinetic limitations, Atmospheric Chemistry and Physics, 9,
794 9491-9522, 2009.
795 Miyazaki, Y., Jung, J., Fu, P., Mizoguchi, Y., Yamanoi, K., and Kawamura, K.: Evidence of formation
796 of submicrometer water-soluble organic aerosols at a deciduous forest site in northern Japan in
797 summer, Journal of Geophysical Research: Atmospheres, 117, n/a-n/a, 10.1029/2012jd018250,
798 2012.

https://doi.org/10.5194/acp-2020-428
Preprint. Discussion started: 29 May 2020


Atmospheric Chemistry and Physics Discussions

799 Müller, L., Reinnig, M. C., Naumann, K. H., Saathoff, H., Mentel, T. F., Donahue, N. M., and
800 Hoffmann, T.: Formation of 3-methyl-1,2,3-butanetricarboxylic acid via gas phase oxidation of
801 pinonic acid – a mass spectrometric study of SOA aging, Atmospheric Chemistry and Physics,
802 12, 1483-1496, 10.5194/acp-12-1483-2012, 2012.
803 Mutzel, A., Rodigast, M., Iinuma, Y., Böge, O., and Herrmann, H.: Monoterpene SOA–contribution of
804 first-generation oxidation products to formation and chemical composition, Atmospheric
805 environment, 130, 136-144, 2016.
806 Pajunoja, A., Hu, W., Leong, Y. J., Taylor, N. F., Miettinen, P., Palm, B. B., Mikkonen, S., Collins, D.
807 R., Jimenez, J. L., and Virtanen, A.: Phase state of ambient aerosol linked with water uptake and
808 chemical aging in the southeastern US, Atmospheric Chemistry and Physics, 16, 11163-11176,
809 2016.
810 Parsons, M. T., Knopf, D. A., and Bertram, A. K.: Deliquescence and Crystallization of Ammonium
811 Sulfate Particles Internally Mixed with Water-Soluble Organic Compounds, The Journal of
812 Physical Chemistry A, 108, 11600-11608, 10.1021/jp0462862, 2004.
813 Poschl, U., and Shiraiwa, M.: Multiphase chemistry at the atmosphere-biosphere interface influencing
814 climate and public health in the anthropocene, Chem Rev, 115, 4440-4475, 10.1021/cr500487s,
815 2015.
816 Praplan, A. P., Barmet, P., Dommen, J., and Baltensperger, U.: Cyclobutyl methyl ketone as a model
817 compound for pinonic acid to elucidate oxidation mechanisms, Atmospheric Chemistry and
818 Physics, 12, 10749-10758, 10.5194/acp-12-10749-2012, 2012.
819 Reid, J. P., Bertram, A. K., Topping, D. O., Laskin, A., Martin, S. T., Petters, M. D., Pope, F. D., and
820 Rovelli, G.: The viscosity of atmospherically relevant organic particles, Nat Commun, 9, 956,
821 10.1038/s41467-018-03027-z, 2018.
822 Renbaum-Wolff, L., Grayson, J. W., Bateman, A. P., Kuwata, M., Sellier, M., Murray, B. J., Shilling, J.
823 E., Martin, S. T., and Bertram, A. K.: Viscosity of alpha-pinene secondary organic material and
824 implications for particle growth and reactivity, Proc Natl Acad Sci U S A, 110, 8014-8019,
825 10.1073/pnas.1219548110, 2013.
826 Rudich, Y., Donahue, N. M., and Mentel, T. F.: Aging of organic aerosol: Bridging the gap between
827 laboratory and field studies, Annual Review of Physical Chemistry, 58, 321-352,
828 10.1146/annurev.physchem.58.032806.104432, 2007.
829 Sato, K., Jia, T., Tanabe, K., Morino, Y., Kajii, Y., and Imamura, T.: Terpenylic acid and nine-carbon
830 multifunctional compounds formed during the aging of β-pinene ozonolysis secondary organic
831 aerosol, Atmospheric Environment, 130, 127-135, 10.1016/j.atmosenv.2015.08.047, 2016.
832 Saukko, E., Lambe, A. T., Massoli, P., Koop, T., Wright, J. P., Croasdale, D. R., Pedernera, D. A.,
833 Onasch, T. B., Laaksonen, A., Davidovits, P., Worsnop, D. R., and Virtanen, A.: Humidity-
834 dependent phase state of SOA particles from biogenic and anthropogenic precursors,
835 Atmospheric Chemistry and Physics, 12, 7517-7529, 10.5194/acp-12-7517-2012, 2012.
836 Seaver, M., Galloway, A., and Manuccia, T. J.: Acoustic levitation in a free-jet wind tunnel, Review of
837 Scientific Instruments, 60, 3452-3459, 10.1063/1.1140492, 1989.
838 Seng, S., Guo, F., Tobon, Y. A., Ishikawa, T., Moreau, M., Ishizaka, S., and Sobanska, S.:
839 Deliquescence behavior of photo-irradiated single NaNO3 droplets, Atmospheric Environment,
840 183, 33-39, 10.1016/j.atmosenv.2018.04.007, 2018.

https://doi.org/10.5194/acp-2020-428
Preprint. Discussion started: 29 May 2020


Atmospheric Chemistry and Physics Discussions

841 Shiraiwa, M., Li, Y., Tsimpidi, A. P., Karydis, V. A., Berkemeier, T., Pandis, S. N., Lelieveld, J., Koop,
842 T., and Poschl, U.: Global distribution of particle phase state in atmospheric secondary organic
843 aerosols, Nat Commun, 8, 15002, 10.1038/ncomms15002, 2017.
844 Shrivastava, M., Easter, R. C., Liu, X., Zelenyuk, A., Singh, B., Zhang, K., Ma, P.-L., Chand, D., Ghan,
845 S., Jimenez, J. L., Zhang, Q., Fast, J., Rasch, P. J., and Tiitta, P.: Global transformation and fate
846 of SOA: Implications of low-volatility SOA and gas-phase fragmentation reactions, Journal of
847 Geophysical Research: Atmospheres, 120, 4169-4195, 10.1002/2014jd022563, 2015.
848 Shrivastava, M., Cappa, C. D., Fan, J., Goldstein, A. H., Guenther, A. B., Jimenez, J. L., Kuang, C.,
849 Laskin, A., Martin, S. T., Ng, N. L., Petaja, T., Pierce, J. R., Rasch, P. J., Roldin, P., Seinfeld, J.
850 H., Shilling, J., Smith, J. N., Thornton, J. A., Volkamer, R., Wang, J., Worsnop, D. R., Zaveri,
851 R. A., Zelenyuk, A., and Zhang, Q.: Recent advances in understanding secondary organic
852 aerosol: Implications for global climate forcing, Reviews of Geophysics, 55, 509-559,
853 10.1002/2016rg000540, 2017.
854 Slade, J. H., Ault, A. P., Bui, A. T., Ditto, J. C., Lei, Z., Bondy, A. L., Olson, N. E., Cook, R. D.,
855 Desrochers, S. J., Harvey, R. M., Erickson, M. H., Wallace, H. W., Alvarez, S. L., Flynn, J. H.,
856 Boor, B. E., Petrucci, G. A., Gentner, D. R., Griffin, R. J., and Shepson, P. B.: Bouncier
857 Particles at Night: Biogenic Secondary Organic Aerosol Chemistry and Sulfate Drive Diel
858 Variations in the Aerosol Phase in a Mixed Forest, Environ Sci Technol, 53, 4977-4987,
859 10.1021/acs.est.8b07319, 2019.
860 Song, M., Maclean, A. M., Huang, Y., Smith, N. R., Blair, S. L., Laskin, J., Laskin, A., DeRieux, W.-S.
861 W., Li, Y., Shiraiwa, M., Nizkorodov, S. A., and Bertram, A. K.: Liquid–liquid phase separation
862 and viscosity within secondary organic aerosol generated from diesel fuel vapors, Atmospheric
863 Chemistry and Physics, 19, 12515-12529, 10.5194/acp-19-12515-2019, 2019.
864 Song, Y. C., Haddrell, A. E., Bzdek, B. R., Reid, J. P., Bannan, T., Topping, D. O., Percival, C., and
865 Cai, C.: Measurements and predictions of binary component aerosol particle viscosity, The
866 Journal of Physical Chemistry A, 120, 8123-8137, 2016.
867 Srivastava, D., Favez, O., Perraudin, E., Villenave, E., and Albinet, A.: Comparison of Measurement-
868 Based Methodologies to Apportion Secondary Organic Carbon (SOC) in PM2.5: A Review of
869 Recent Studies, Atmosphere, 9, 10.3390/atmos9110452, 2018.
870 Sun, J., Liu, L., Xu, L., Wang, Y., Wu, Z., Hu, M., Shi, Z., Li, Y., Zhang, X., Chen, J., and Li, W.: Key
871 Role of Nitrate in Phase Transitions of Urban Particles: Implications of Important Reactive
872 Surfaces for Secondary Aerosol Formation, Journal of Geophysical Research: Atmospheres,
873 123, 1234-1243, 10.1002/2017jd027264, 2018.
874 Szmigielski, R., Surratt, J. D., Gómez-González, Y., Van der Veken, P., Kourtchev, I., Vermeylen, R.,
875 Blockhuys, F., Jaoui, M., Kleindienst, T. E., Lewandowski, M., Offenberg, J. H., Edney, E. O.,
876 Seinfeld, J. H., Maenhaut, W., and Claeys, M.: 3-methyl-1,2,3-butanetricarboxylic acid: An
877 atmospheric tracer for terpene secondary organic aerosol, Geophysical Research Letters, 34,
878 10.1029/2007gl031338, 2007.
879 Tang, M., Chan, C. K., Li, Y. J., Su, H., Ma, Q., Wu, Z., Zhang, G., Wang, Z., Ge, M., Hu, M., He, H.,
880 and Wang, X.: A review of experimental techniques for aerosol hygroscopicity studies,
881 Atmospheric Chemistry and Physics, 19, 12631-12686, 10.5194/acp-19-12631-2019, 2019.

https://doi.org/10.5194/acp-2020-428
Preprint. Discussion started: 29 May 2020


Atmospheric Chemistry and Physics Discussions

882 Topping, D., Connolly, P., and McFiggans, G.: Cloud droplet number enhanced by co-condensation of
883 organic vapours, Nature Geoscience, 6, 443, 2013.
884 Virtanen, A., Joutsensaari, J., Koop, T., Kannosto, J., Yli-Pirilä, P., Leskinen, J., Mäkelä, J. M.,
885 Holopainen, J. K., Pöschl, U., and Kulmala, M.: An amorphous solid state of biogenic secondary
886 organic aerosol particles, Nature, 467, 824, 2010.
887 Vlachou, A., Tobler, A., Lamkaddam, H., Canonaco, F., Daellenbach, K. R., Jaffrezo, J.-L., Minguillón,
888 M. C., Maasikmets, M., Teinemaa, E., Baltensperger, U., El Haddad, I., and Prévôt, A. S. H.:
889 Development of a versatile source apportionment analysis based on positive matrix
890 factorization: a case study of the seasonal variation of organic aerosol sources in Estonia,
891 Atmospheric Chemistry and Physics, 19, 7279-7295, 10.5194/acp-19-7279-2019, 2019.
892 Vogel, A. L., Äijälä, M., Corrigan, A. L., Junninen, H., Ehn, M., Petäjä, T., Worsnop, D. R., Kulmala,
893 M., Russell, L. M., Williams, J., and Hoffmann, T.: In situ submicron organic aerosol
894 characterization at a boreal forest research station during HUMPPA-COPEC 2010 using soft and
895 hard ionization mass spectrometry, Atmospheric Chemistry and Physics, 13, 10933-10950,
896 10.5194/acp-13-10933-2013, 2013.
897 Wang, B., O'Brien, R. E., Kelly, S. T., Shilling, J. E., Moffet, R. C., Gilles, M. K., and Laskin, A.:
898 Reactivity of liquid and semisolid secondary organic carbon with chloride and nitrate in
899 atmospheric aerosols, J Phys Chem A, 119, 4498-4508, 10.1021/jp510336q, 2015.
900 Wang, X., Jing, B., Tan, F., Ma, J., Zhang, Y., and Ge, M.: Hygroscopic behavior and chemical
901 composition evolution of internally mixed aerosols composed of oxalic acid and ammonium
902 sulfate, Atmospheric Chemistry and Physics, 17, 12797-12812, 10.5194/acp-17-12797-2017,
903 2017.
904 Wang, Z., Jing, B., Shi, X., Tong, S., Wang, W., and Ge, M.: Importance of water-soluble organic acid
905 on the hygroscopicity of nitrate, Atmospheric Environment, 190, 65-73,
906 10.1016/j.atmosenv.2018.07.010, 2018.
907 Wu, L., Li, X., Kim, H., Geng, H., Godoi, R. H. M., Barbosa, C. G. G., Godoi, A. F. L., Yamamoto, C.
908 I., de Souza, R. A. F., Pöhlker, C., Andreae, M. O., and Ro, C.-U.: Single-particle
909 characterization of aerosols collected at a remote site in the Amazonian rainforest and an urban
910 site in Manaus, Brazil, Atmospheric Chemistry and Physics, 19, 1221-1240, 10.5194/acp-19-
911 1221-2019, 2019a.
912 Wu, L., Li, X., and Ro, C.-U.: Hygroscopic Behavior of Ammonium Sulfate, Ammonium Nitrate, and
913 their Mixture Particles, Asian Journal of Atmospheric Environment, 13, 196-211,
914 10.5572/ajae.2019.13.3.196, 2019b.
915 Wu, Z. J., Nowak, A., Poulain, L., Herrmann, H., and Wiedensohler, A.: Hygroscopic behavior of
916 atmospherically relevant water-soluble carboxylic salts and their influence on the water uptake
917 of ammonium sulfate, Atmospheric Chemistry and Physics, 11, 12617-12626, 10.5194/acp-11-
918 12617-2011, 2011.
919 Yasmeen, F., Szmigielski, R., Vermeylen, R., Gomez-Gonzalez, Y., Surratt, J. D., Chan, A. W.,
920 Seinfeld, J. H., Maenhaut, W., and Claeys, M.: Mass spectrometric characterization of isomeric
921 terpenoic acids from the oxidation of alpha-pinene, beta-pinene, d-limonene, and Delta3-carene
922 in fine forest aerosol, J Mass Spectrom, 46, 425-442, 10.1002/jms.1911, 2011.

https://doi.org/10.5194/acp-2020-428
Preprint. Discussion started: 29 May 2020


Atmospheric Chemistry and Physics Discussions

923 Yatavelli, R. L. N., Mohr, C., Stark, H., Day, D. A., Thompson, S. L., Lopez-Hilfiker, F. D.,
924 Campuzano-Jost, P., Palm, B. B., Vogel, A. L., Hoffmann, T., Heikkinen, L., Äijälä, M., Ng, N.
925 L., Kimmel, J. R., Canagaratna, M. R., Ehn, M., Junninen, H., Cubison, M. J., Petäjä, T.,
926 Kulmala, M., Jayne, J. T., Worsnop, D. R., and Jimenez, J. L.: Estimating the contribution of
927 organic acids to northern hemispheric continental organic aerosol, Geophysical Research
928 Letters, 42, 6084-6090, 10.1002/2015gl064650, 2015.
929 Zhang, Y. Y., Müller, L., Winterhalter, R., Moortgat, G. K., Hoffmann, T., and Pöschl, U.: Seasonal
930 cycle and temperature dependence of pinene oxidation products, dicarboxylic acids and
931 nitrophenols in fine and coarse air particulate matter, Atmospheric Chemistry and Physics, 10,
932 7859-7873, 10.5194/acp-10-7859-2010, 2010.
933
934
935
936
937

https://doi.org/10.5194/acp-2020-428
Preprint. Discussion started: 29 May 2020

Atmospheric Chemistry and Physics Discussions

Figure 1. Calculated titration curve for MBTCA, noted as H_3M in this figure. The experimental data are shown as orange triangles. 5 mL of 0.02 M H_3M was titrated with a 0.1 M NaOH solution.

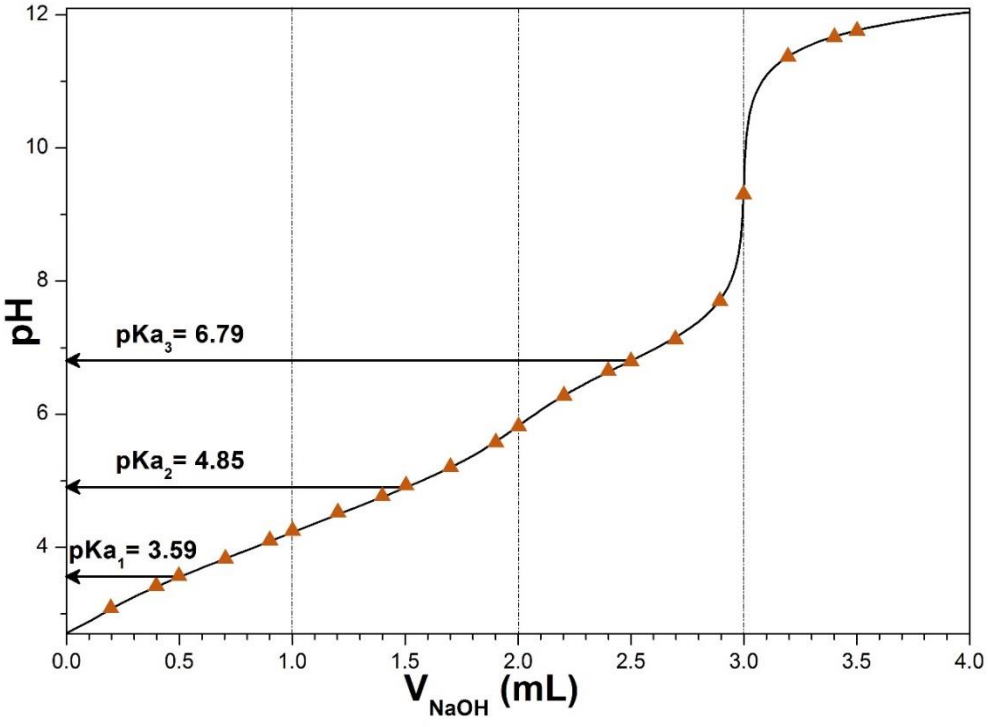

https://doi.org/10.5194/acp-2020-428
Preprint. Discussion started: 29 May 2020

Atmospheric Chemistry and Physics Discussions

947 Figure 2. Hygroscopic curves, corresponding optical images, and Raman spectra at specific RHs of three
948 types of pure MBTCA particles. The transition RHs recorded during the dehydration (D) and
949 humidification (H) processes are marked with arrows in the hygroscopic curves.
950
951

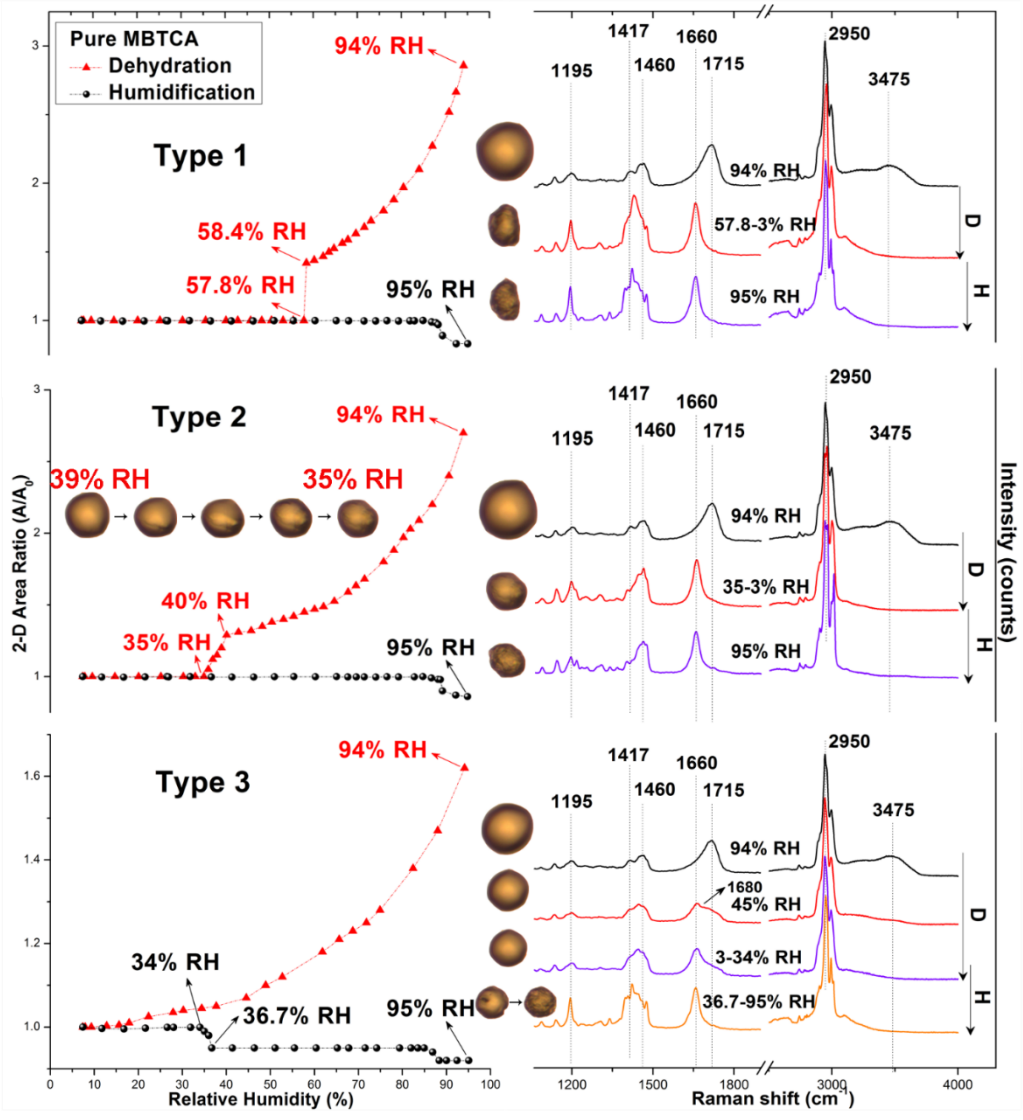

https://doi.org/10.5194/acp-2020-428
Preprint. Discussion started: 29 May 2020

Atmospheric Chemistry and Physics Discussions

952 Figure 3. Hygroscopic curves, corresponding optical images, and Raman spectra at specific RHs of (a)
953 mono-, (b) di-, and (c) tri-sodium MBTCA salt aerosols. The recorded transition RHs during the
954 dehydration and humidification processes are marked with arrows in the hygroscopic curves.
955
956

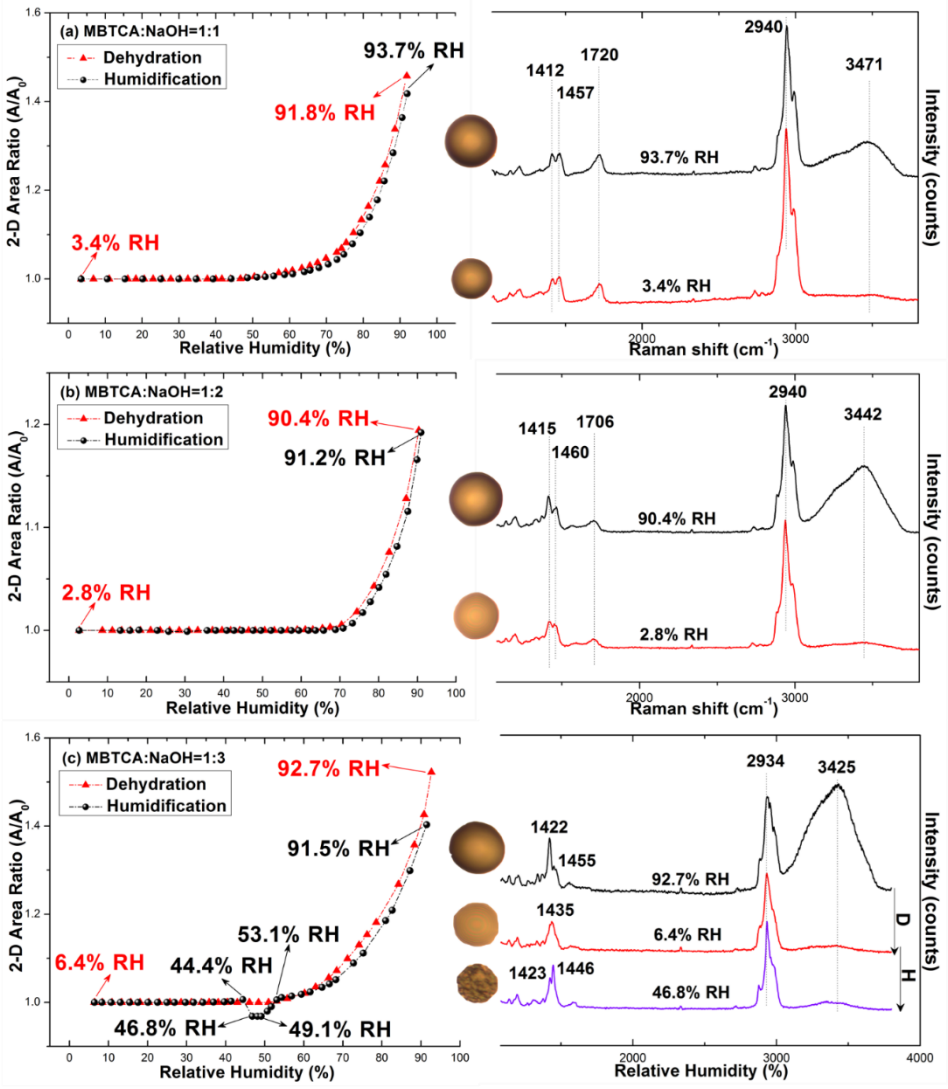

https://doi.org/10.5194/acp-2020-428
Preprint. Discussion started: 29 May 2020

Atmospheric Chemistry and Physics Discussions

Figure 4. Hygroscopic curves, corresponding optical images, and Raman spectra at specific RHs of MBTCA:NaCl = (a) 1:1 and (b) 2:1. The recorded transition RHs during the dehydration (D) and humidification (H) processes and the chemical compositions of the mixtures at certain RHs are marked with arrows in the hygroscopic curves. The phase notations shown in parenthesis are s=solid; aq=aqueous; and as=amorphous solid.

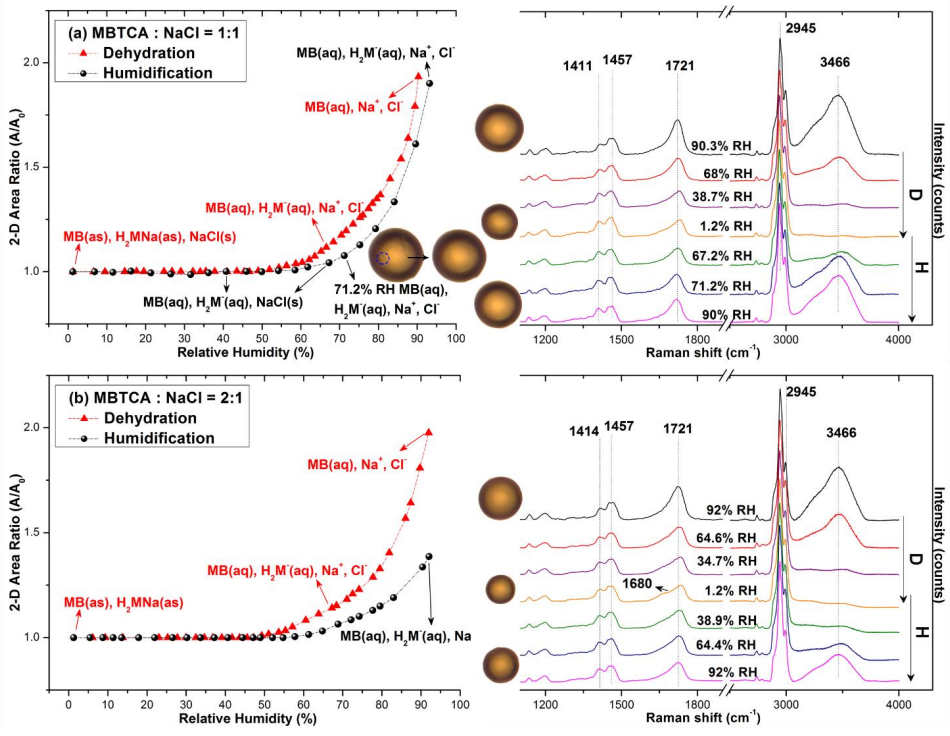

https://doi.org/10.5194/acp-2020-428
Preprint. Discussion started: 29 May 2020

Atmospheric Chemistry and Physics Discussions

Figure 5. Hygroscopic curves, corresponding optical images, and Raman spectra at specific RHs of MBTCA:NaCl = (a) 1:2 and (b) 1:3. The recorded transition RHs during the dehydration (D) and humidification (H) processes and the chemical compositions of the mixtures at certain RHs are marked with arrows in the hygroscopic curves. The phase notations shown in parenthesis are s=solid; aq=aqueous; and as=amorphous solid.

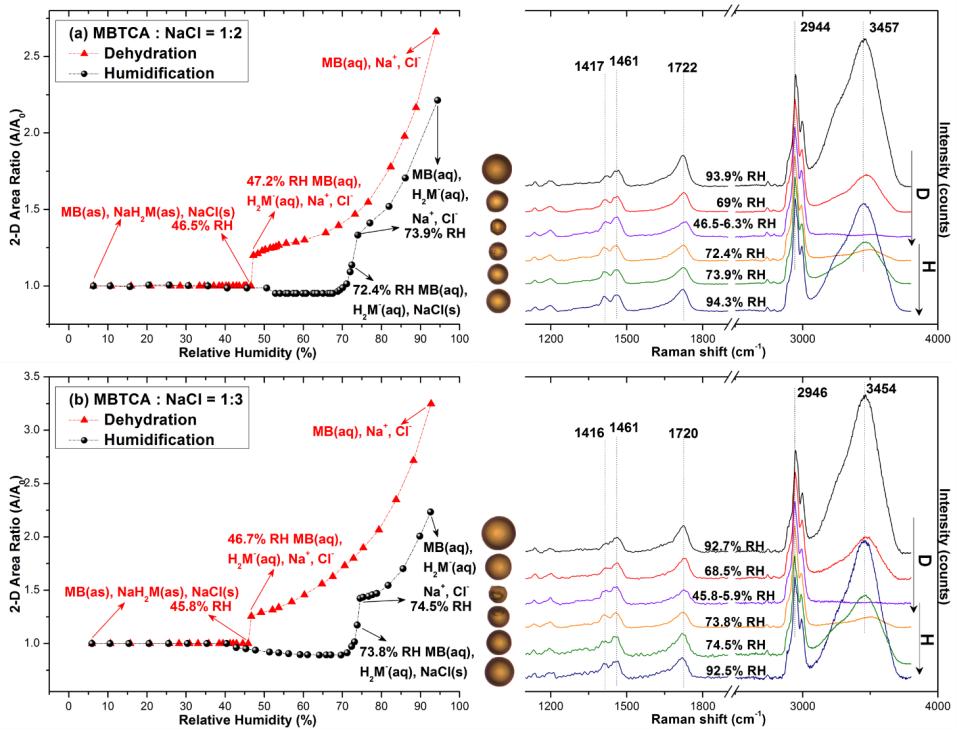

https://doi.org/10.5194/acp-2020-428
Preprint. Discussion started: 29 May 2020

Atmospheric Chemistry and Physics Discussions

967 Figure 6. (a) Raman spectra of pure NaH_2M and mixture aerosols with mixing ratios of MBTCA:NaCl =
968 1:1, 1:2, and 1:3 obtained at the end of the humidification process, which were normalized to the CH_3
969 peak at 1458 cm^{-1} and (b) Raman spectra of pure MBTCA, mixture of MBTCA:NaH_2M = 1:1, and pure
970 NaH_2M, which are normalized to the CH_3 peak at 1460 cm^{-1}.
971
972

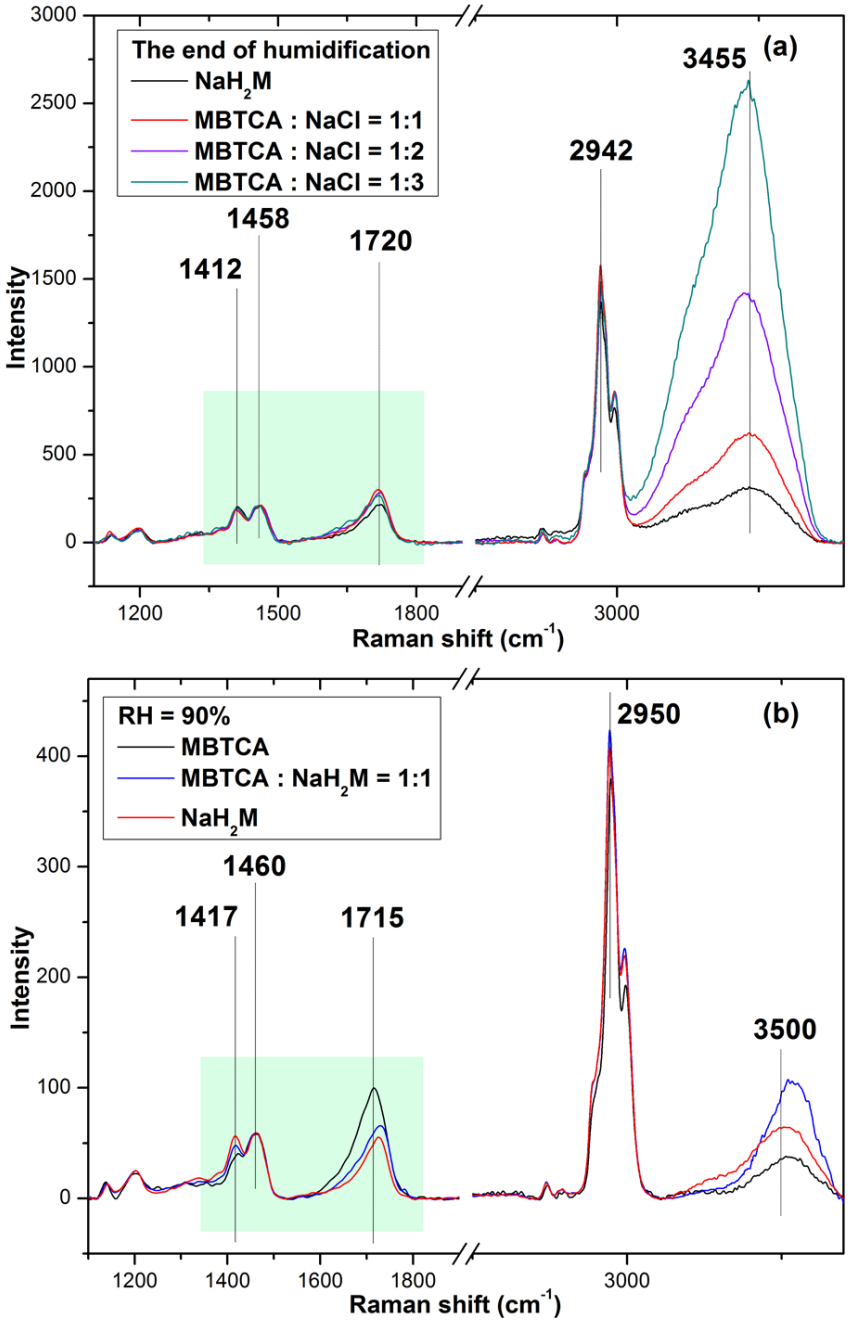

https://doi.org/10.5194/acp-2020-428
Preprint. Discussion started: 29 May 2020

Atmospheric Chemistry and Physics Discussions

973 Figure 7. (a) Calibration curve calculated from the intensity ratios of two peaks at 1460 and 1720 cm^{-1} as
974 a function of RH for NaH_2M, MBTCA:NaH_2M = 1:1, and MBTCA aerosols; (b) chemical reactivity
975 represented as the degree of reaction for mixture aerosols of MBTCA:NaCl = 1:1, 1:2, 1:3, and 2:1 during
976 the dehydration and humidification processes.
977
978

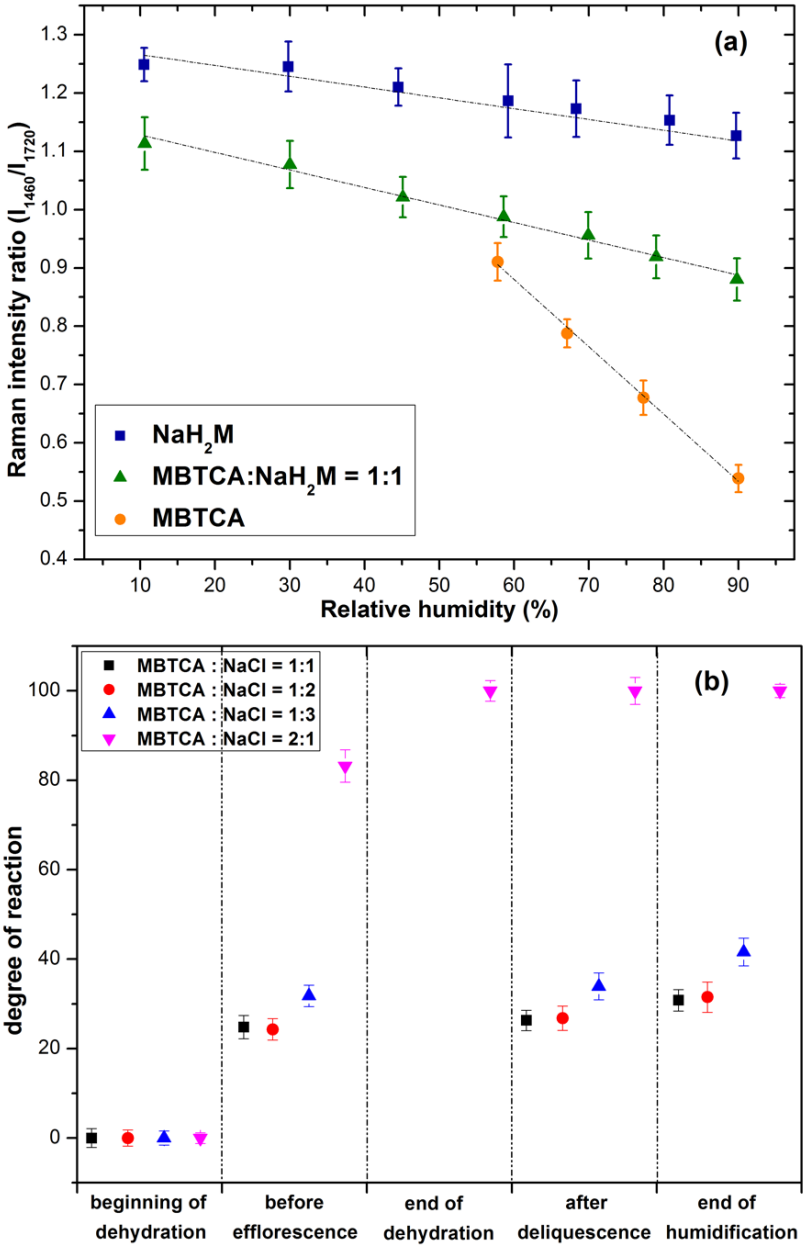

https://doi.org/10.5194/acp-2020-428
Preprint. Discussion started: 29 May 2020

Atmospheric Chemistry and Physics Discussions

Figure 8. (a) Secondary electron images (SEIs) and elemental X-ray maps for C (from MBTCA and NaH_2M), Na (from NaH_2M and NaCl), and Cl (from NaCl). The scale bars are for 5 μm; (b) X-ray spectra and elemental concentrations of particles with four mixing ratios.